SCUOLA DI SCIENZE

Dipartimento di Chimica Industriale "Toso Montanari"

Corso di Laurea Magistrale in

Chimica Industriale

Classe LM-71 - Scienze e Tecnologie della Chimica Industriale

Preparation and Characterization of Polymeric Beads and Membranes for Boron Removal From Water

Tesi di laurea sperimentale

CANDIDATO

Alessandro Fabbri

RELATORE

Chiar.mo Prof. Daniele Caretti

CORRELATORI

Prof.ssa Ana Aguiar-Ricardo

Prof.ssa Teresa Casimiro

Dott.ssa Raquel Viveiros

List of contents

1. Introduction

In perspective of the demographic growth we are going to face in next years, one of the main challenges for humanity will be the availability of needful and indispensable resources for human and vegetal life, especially water. In certain areas of the planet, despite being present in large quantity, water is not suitable for human consumption due to pollutants, toxic, or salty elements. Water purification techniques have therefore assumed higher relevance, in perspective of the need to use unconventional water sources.

In particular, the necessity for boron separation and recovery from aqueous streams derives not only from human health issues, but also from the growing demand for his industrial applications, the production of freshwater from seawater and the purification of waste streams such as natural gas brines[1].

For this purpose, the most promising technique is reverse osmosis (RO) which is also able to produce desalinized water from seawater by simply passing the stream to be treated through a proper membrane applying high pressures. Nevertheless, this technique is not able to remove with an affordable cost boric acid, which is present in a modest quantity in seawater, making RO treated water unapt for human and agricultural consumption unless a pre-treatment system is included in the process.

State-of-the-art pre-treatment systems consist mainly in boron adsorbents; nevertheless, they are not able to achieve satisfactory results, due to issues such as low selectivity, low capacity of adsorption, slow kinetic.

1.1. Boron

Boron is a metalloid element with atomic number equal to 5 and symbol B. The stable isotopes of B have mass of 10 and 11 Da and are present in an approximate 20:80% ratio to afford an atomic weight of 10.81 Da.

The principal industrial uses of boron compounds are in the production of fiberglass, heat resistant borosilicate glass (e.g. Pyrex) and detergents. Boron is also used in fertilisers and herbicides, in metallurgy and nuclear shielding.

Boron does not occur in the elemental form in nature, and it is mostly encountered in ground and seawater as boric acid or bounded to oxygen atoms to form borates minerals. It is widely distributed in both hydrosphere and lithosphere: in seawater it can be found in a concentration range that varies from 1 to 10 mg/L, while soils are usually divided into two types: those with low B content (<10 mg/Kg) and those with high B content (10 to 100 mg/Kg), the latter often associated with recent volcanism.

Boron is a bioactive beneficial element at low concentrations[2]: in human beings, it influences a variety of biological reactions and interacts with calcium and vitamin D accumulating in bones[3], stabilizes ribose, which is a constituent of RNA and is able to influence the metabolism of many substances involved in growth and development[4]. Moreover, low boron concentration has been related with poor immune function, increased risk of mortality, osteoporosis, and cognitive deterioration[5].

Nevertheless, high levels of exposure to boron can be dangerous and cause several diseases such as damage to the nervous system and inhibition of fertility[6]. WHO guideline assesses that boron concentration in drinking water should not be higher than 2.4 mg/L[7]. Anyway, the guideline is designed as provisional because in certain areas it is difficult to achieve. In fact, at present, treatment technologies for boron removal are either very expensive or incapable of cut down to the concentration required.

1.1.1. Boric acid speciation in solution

Boron can be found in solution almost exclusively as boric acid.

The aforementioned species behaves as a very weak Lewis acid (pK_a=9.1 K_a=6×10^{-10}) according to the *Equation 1*:

$$B(OH)_3 + H_2O \leftrightarrow B(OH)_4^- + H^+ \quad (1)$$
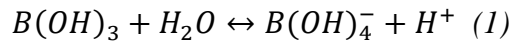
As it can be noted on the diagram in *Figure 1*, when pH is below pK_a of boric acid accepts a hydroxide ion, releasing a proton, while in alkaline aqueous solutions, boric acid transform to monoborate anion.
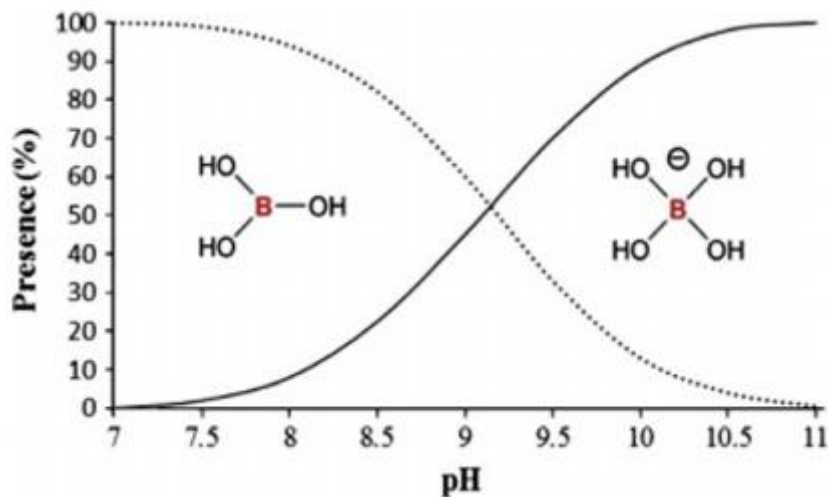
Figure 1: Distribution diagram of boric acid and borate ion to changes in pH.
The graphic was taken from GUAN, Zhimin, et al. Boron removal from aqueous
solutions by adsorption—A review. Desalination, 2016, 383: 29-37.

At low concentration (<0,02M) only the molecular species $B(OH)_3$ and $B(OH)_4^-$ are present. Nevertheless, at higher concentrations polynuclear species such as $B_2O(OH)_6^{2-}$ or B_3O_3 rings start to form[8].

For what it may concern this thesis, it is relevant to report the interaction of boron with alcohols. Boric acid reacts with hydroxyl groups according to *Equation 2* forming borate esters:

$$B(OH)_3 + 3ROH \leftrightarrow B(OR)_3 + 3H_2O \quad (2)$$
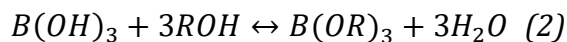
The reaction reported above may also happen with polyols[9] (e.g. mannitol, sorbitol, meglumine), namely molecules containing more than one alcoholic functionality, giving origin to chelate complexes. In the specific, as can be noted in *Figure 2,* during the reaction of boric acid with protonated alcohols the characteristic transition step involves proton transfer from the entering ligand group of the polyol to the boric acid –OH acting as a leaving group.
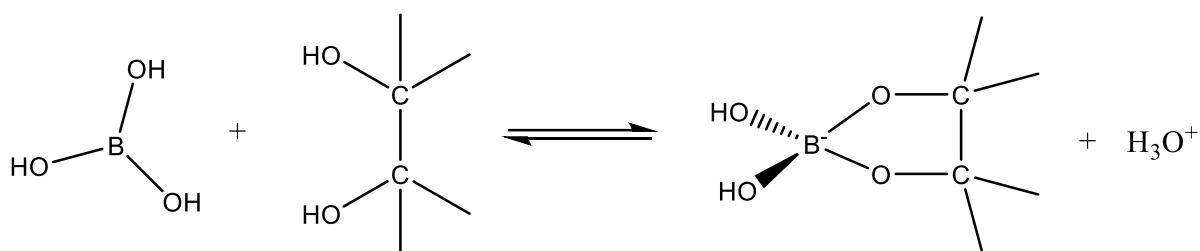
Figure 2: Boric acid reaction with polyols

The pH of the solution assumes fundamental importance in determining the equilibrium of the reaction. As an exemplification in *Figure 3* is reported the distribution diagram for boric acid/lactic acid complexes formation made by *Pizer*[9].

It can be noted that, if pH < 2 boron is encountered as boric acid and no complex is formed due to the abundance of protons shifting the equilibrium towards the reagents. When pH > 10 boron is mostly in the form of borate anion $B(OH)_4^-$ and again no complex is formed.

The highest concentration of monochelate complex is found at a neutral range of pH, when the prevalent specie in water is boric acid and the H_3O^+ ion concentration is not high enough to push the reaction backwards.
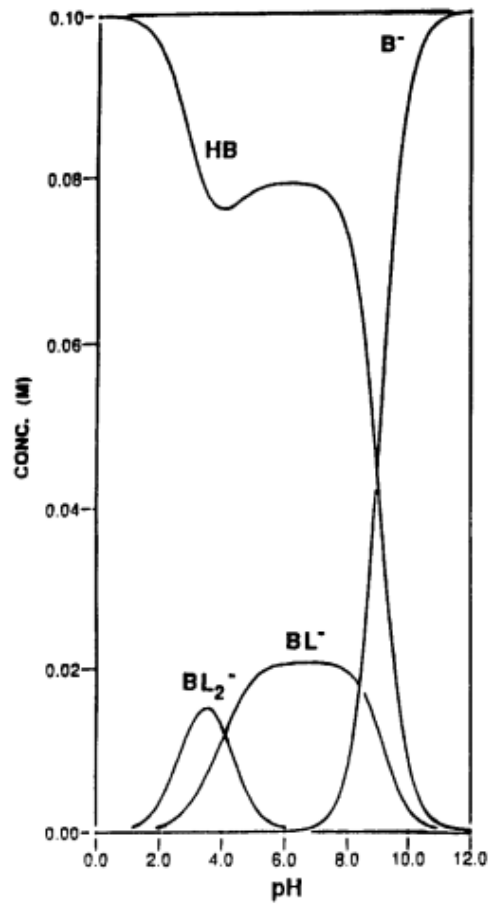
Figure 3: Concentration of boric acid/lactic acid complexes by changes in pH. HB= boric acid; B-=borate ion; BL-=monochelate complex; BL2-=bischelate complex.

1.1.2. Boric acid and N-methyl-D-glucamine interaction
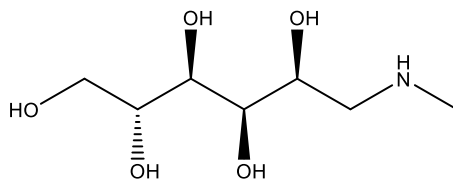
Figure 4: N-methyl-D-glucamine chemical structure.

Amongst the sugars and polyols able to form complexes with boron, N-methyl-D-glucamine (NMDG) is certainly the most studied. As it can be seen in *Figure 4* NMDG is an amino-sugar derived from glucose possessing five hydroxyl groups.

NMDG exhibits an enhanced complexation capability compared to other sugars such as D-mannitol or D-sorbitol, due to different reasons. First of all the molecular structure allows NMDG to arrange in a way that the OH groups match the structural parameters required to coordinate a boron atom. *Yoshimura et al.*[10] proposed that the structure of chelate complexes between boron and NMDG that form in aqueous solution may be monochelate, tetradentate or bischelate (*Figure 5*).

The mechanism of complexation reaction of boric acid and NMDG is illustrated in *Figure 5*. It is similar to the one reported in *Figure 2* with the addition of a further step:

      a) complexation of borate ion by two alcoholic groups with consequent release of protons in solution. In fact, one of the alcoholic groups react throughout a condensation mechanism, producing one H_2O molecule, while the other reacts with a nucleophile substitution mechanism;

      b) proton capture by tertiary amine sites that behave as weakly basic anion exchangers.

Further reasons determining stronger interaction between boric acid and NMDG moieties than boric acid with other polyols are:

-the presence of step b: the consecutive reaction removes the product of the first step, shifting the thermodynamic equilibrium more towards the complex formation. The mechanism is not

pure ion exchange; the presence of nitrogen atoms acting as a buffer avoids pH value decrease and subtracts H_3O^+ ions from the equilibrium, thus favouring the complex formation

-the electrostatic attraction between protonated amino-group and borate anion, which stabilizes the complex.

monochelate complex   tetradentate complex   bischelate complex
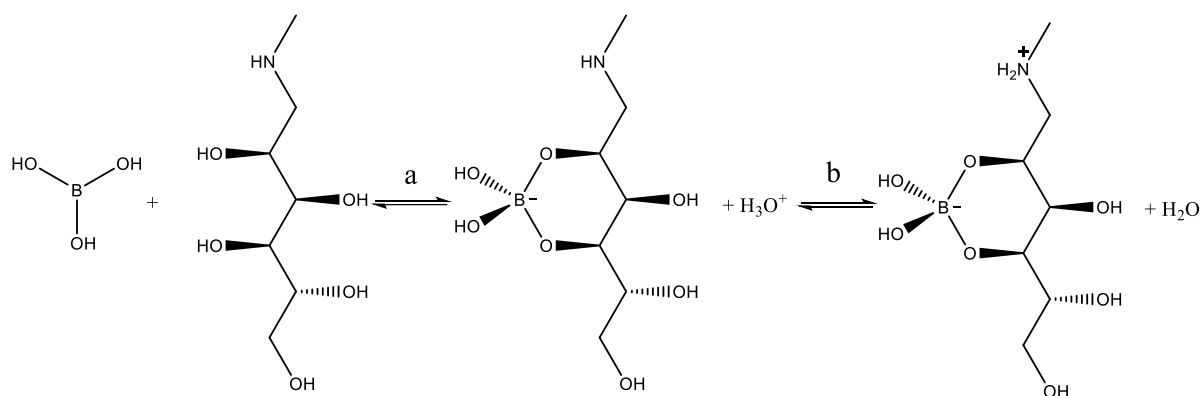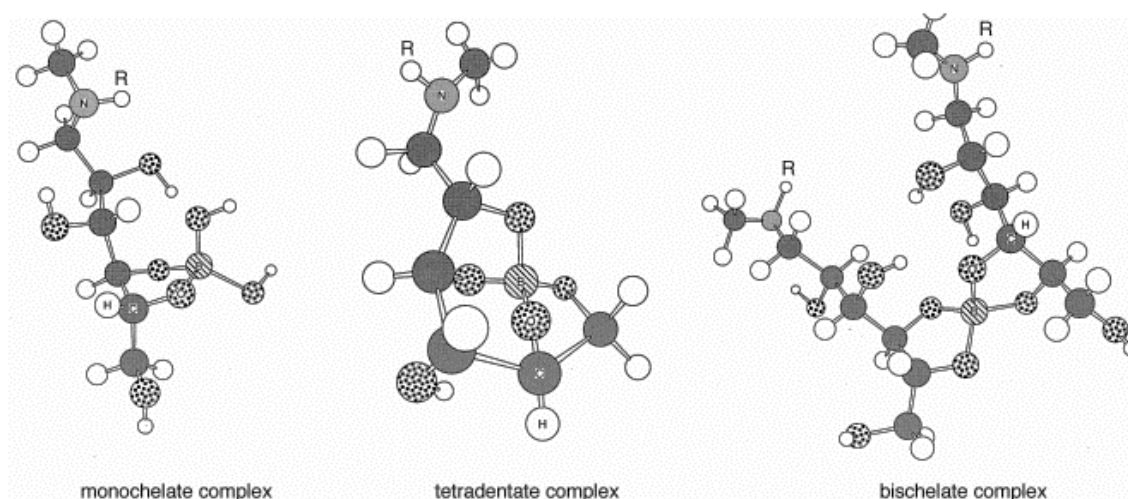

Figure 5: Schematic representation of different possible binding interactions between boron and NMDG (top) and reaction scheme for the monochelate complex formation (bottom).

1.2. Water treatment systems for boron removal

Amongst the wide number of techniques used for water purification, the most common and effective are: membrane processes (e.g. reverse osmosis), ionic exchange, adsorption, and electrodialysis. As a matter of facts, the characteristics that make a separation system more valuable are the specific capacity and selectivity, time required for the treatment, cost and reusability.

Concerning boron removal from water, the techniques commonly used can be divided in two groups:

-separation by adsorption on solid
-separation by membrane filtration
Hybrid techniques using a combination of the two approaches have also found application.

1.2.1. Separation by adsorption on solids

The first adsorption techniques proposed involved chemical and physical adsorption of boric acid onto in-situ originated solids[11,12], or on activated carbon, alumina or bauxite[13]. However, even possessing a good adsorption capability, the aforementioned techniques are not apt for industrial application due to the incapability of regeneration of the sludge formed or the slow kinetic of adsorption.

Removal processes based on regenerable adsorbents in the form of packed columns have therefore been considered in order to minimize apparatus footprint and amount of solid waste. In this context, in order to compare different techniques, additional sorbent key properties must be taken into account: effectiveness of regeneration (loss of properties after different cycles should be minimum) and chemical and mechanical stability under operational conditions.

Commercially available products based on polymeric matrixes of styrene-divinylbenzene upon which is grafted dimethylethanolbenzylammonium chloride (Dowex 2X8) or NMDG

(Amberlite IRA743) can undergo regeneration with a two-step process involving acid washing to elute boric acid and subsequently basic washing to regenerate the functionalities. Nevertheless Dowex BSR-1[14] resin possess small selectivity and long kinetic, while adsorption capability of 3.1 mg/g of Amberlite IRA743[15] is not as good as some of the other sorbents tested at lab scale.

In particular, the best results on laboratory scale were obtained by *Wei et al.*[16]. They grafted NMDG on surface activated chitosan beads obtaining on a batch test an absorption of 30 mg/g. A similar study carried out by *Sabarudin et al.*[17] reports the production of cross-linked chitosan beads with a sorption capability of 21 mg/g. Unfortunately, in both cases the reactions needed to functionalize chitosan are not only expensive to carry out, but also in disagreement with the green chemistry principles, due to the involvement of protection-deprotection steps in the synthetic pathway and the use of organic solvents such as tetrahydrofuran and dimethyl formammide. Therefore, the aforementioned devices are not applicable on industrial scale.

1.2.2. Membrane filtration

Membranes are defined as semipermeable films of organic or inorganic materials able to selectively separate a fluid from its components in solution or in suspension if external work is applied. Depending on the porosity of the membrane and the pressure applied, filtration techniques can be divided into 4 main categories, illustrated in *Figure 6*. Reverse osmosis (RO) is widely recognized as one of the most important technologies for freshwater production from saline water and wastewater. A schematic representation of RO mechanism of action is provided in *Figure 7*. Applying a hydrostatic pressure, which can vary from 250 to 400 psi or 800 to 1000 psi for brackish water and seawater respectively, the osmotic pressure is overcome and the fluid to process permeates through a semipermeable or impermeable membrane possessing a well-defined structure.

The process allows water molecules to pass and cuts off bigger molecules, thus retaining most of salt ions[18] in the high pressure side of the membrane. Contrarily from the others filtration techniques, RO mechanism for retention is not size exclusion but solvent diffusion throughout a non-porous membrane or a nano-porous membrane.
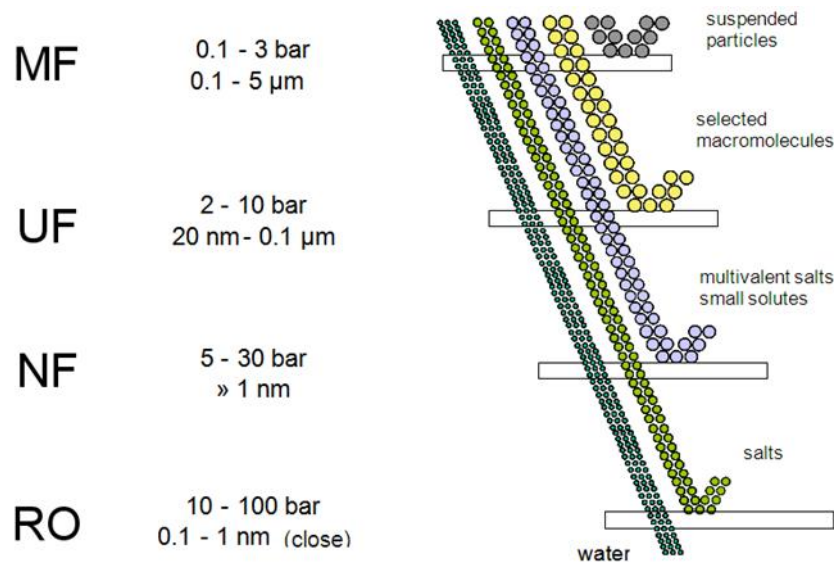
Figure 6: Pressure and pore size ranges characterizing the different techniques of filtration: MF=microfiltration; UF=ultrafiltration; NF=nanofiltration, RO=reverse osmosis

One of the biggest issues concerning RO is boron removal. The effectiveness of RO in separating boric acid is not satisfactory because the molecule passes through the membrane almost as easily as water does due to different aspects:

-small size of the neutral molecule;

-absence of electrostatic charges;

-tendency to hydrogen bonding with the membrane polymeric matrix.

For this reason one passage of seawater through a RO system is just able to achieve a percentage of rejection $< 80\%$[19], which is not enough to comply with the WHO guidelines. Under alkaline conditions (pH > 9) boron is encountered in the form of borate ions, $B(OH)_4^-$ which possess a
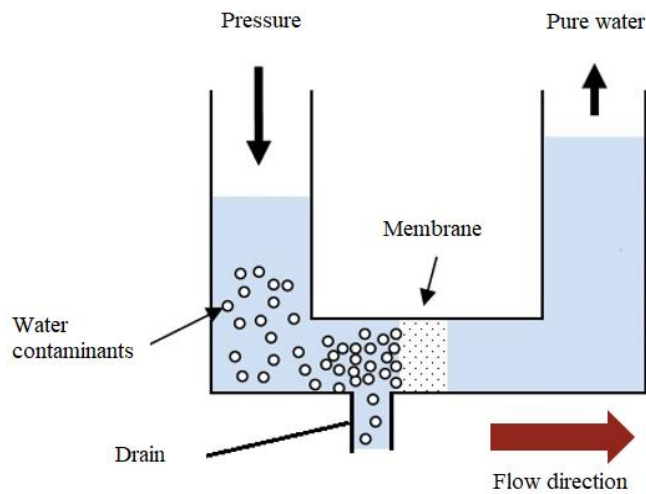
Figure 7: Schematic representation of an RO system.

bigger diameter and more hydration layers than the neutral form. Under these conditions RO membranes are capable of producing boron-free water (rejection percentage $> 99\%$ [20]).

It can be assessed that most of the state-of-the-art RO membranes fail to attain satisfactory boron rejection[21] due to two major drawbacks that narrow RO field of applicability. Firstly, the consumption of chemicals needed to vary the pH is expensive and adds an additional operation unit to the system. In addition to this, the precipitation of calcium and magnesium hydroxides occurring on the membrane surface due to supersaturation at basic pH affects the productivity of the membrane. This effect is commonly known as *"scaling"* phenomena[22].

The most common solution for boron removal using RO plants is to add a pre-treatment column containing a boron selective ion exchange resin after the filtration unit. However, concerns regarding the storage of chemicals for regeneration of the resin, their disposal and high costs represent serious problems still to be resolved[18].

Another interesting technology for boron separation is polymer assisted ultrafiltration (PAUF), consisting in the addition of soluble poly-alcohol macromolecules able to form complexes after reaction with boric acid. Due to his molecular weight (at least 10 kDa), the complex can be retained by an ultrafiltration unit. The polymer is then recovered by complex hydrolysis under acidic conditions.

Compared to RO, membranes used for PAUF possess bigger pores. For this reason, besides being easier to produce, they also require lower pressures to permeate and thus less energy consumption. In fact, the operating pressure range of an ultrafiltration unit is between 30 and 100 psi, much smaller than the RO pressure (250-400 or 800-1000 psi).

Due to the compactness of membrane modules, PAUF has been claimed as a possible alternative to boron selective resins for the treatment of water streams in locations where floor space is expansive (e.g., oil platforms). Nevertheless, PAUF application field is limited by the relatively low boron concentrations they are able to remove.[23]

Adsorption membrane filtration (AMF) is an example of technique combining adsorption on solids and membrane filtration. In this case, the solid adsorbent is suspended in the aqueous stream and then separated through membrane filtration. Subsequently the adsorbent is regenerated and recovered in order to be reused. Unfortunately, commercially available boron selective adsorbents are sized for column packing and possess a diameter ranging from 300 to 500 μm, while the required size to implement this technique is around 50 μm. Large scale production of a resin possessing those dimensions is a major challenge for the implementation of this technique[24].

1.3. Supercritical carbon dioxide and its use for the production of porous structures

In the last decades, supercritical fluids (SCF) have become a relevant and efficient alternative to traditional solvents not only from the sustainability of their implementation in industrial plants, but also due to their specific physical, chemical and toxicological characteristics that constitute an advantage owing to the easiness in manipulating the outcome of reactions and processing. A SCF is any substance at a temperature and pressure above its critical point, marked by critical temperature (T_c) and critical pressure (P_c) but below the pressure at which the fluid would solidify. In the supercritical state there are no distinct liquid and gas phases.

A remarkable aspect which gives supercritical fluids unique properties is that they possess viscosity, diffusivity and density values intermediate between the gas and liquid (*Table 1*), which can be readily tuned by small variations in temperature or pressure, especially when the system is in a state close to the critical point.

Table 1: Values range of density, viscosity and diffusivity for gas, supercritical and liquid fluids

	Density (Kg/m^3)	Viscosity(cP)	Diffusivity (mm^2/s)
Gases	1	0.001	1-10
Supercritical	100-1000	0.05-0.1	0.01-0.1
Liquid	1000	0.5-1.0	0.001

Supercritical carbon dioxide ($scCO_2$) is a non-toxic, chemically inert, non-flammable and low cost solvent and thus has found applications in a broad range of areas[25] (e.g. extraction, polymerization, particle design, chemical reactions, drug impregnation, formation of porous structures, dry cleaning). Besides the aforementioned qualities, $scCO_2$ is the most common SCF for industrial process owing to the relatively mild condition at which the supercritical state can be reached compared to other inert SCF (Table 2). In fact, referring to *Table* 2, it can be

observed that the critical point is situated at $T_c=31°C$ and $P_c=72.9$ atm, conditions easily accessible by simple compression and mild heating of the gas. Moreover, gaseous CO_2 can be easily recovered at the end of the process by depressurization and therefore recycled. Moreover patented processes allowing to recover 100% purity CO_2 are available, thus avoiding the purge of a part of the gas and consequently limiting the environmental damage[26].

Table 2: Critical temperature and pressure of various solvents

Solvent	Critical temperature (K)	Critical pressure (MPa)
Carbon dioxide	304.1	7.38
Water	647.3	22.12
Ethane	305.3	4.87
Ethylene	282.4	5.04
Propane	369.8	4.25
Methanol	512.6	8.09
Acetone	508.1	4.7

Besides its environmental advantages, the use of $scCO_2$ in synthesis and processing of polymers allows the production of a dry product[27] because CO_2 is a gas under room conditions and therefore easy to separate, leaving no trace of the solvent. Furthermore, CO_2 utilization introduces additional parameters to control product morphology such as pressure, temperature and depressurization time, accelerates mass transfer owing to his lower viscosity compared to organic liquids, and reduces the solvent recovery costs.

These advantages may have a remarkable impact on process economics and be able to compensate the costs needed to compress the gas and the investments for high pressure resistant equipment. In these cases, $scCO_2$ has been implemented in industrial scale processes, specifically in the field of food processing[28], seed and essential oils extraction[29] and to induce phase transition in polymers[30].

Several SCF-assisted techniques have been used for the preparation of polymeric porous structures. The main processes are: foaming, emulsion templating and CO_2 assisted phase inversion method[31].

1.3.1. Foaming process

Carbon dioxide was first used as a physical-blowing agent in order to process glassy polymers into foam by Martini and co-workers[32]. Foaming process method takes advantage of the large diminution in glass transition temperature (T_g) due to the plasticization effect that $scCO_2$ has on many polymers. The foaming process which is schematized in *Figure 8*[33], takes place when a polymer, after being plasticized and swollen till saturation of the SCF, is rapidly depressurized at a constant temperature.

As pressure is released, CO_2 passes from the supercritical state to the gas state. The gas has lower affinity with the polymer compared to the SCF, and therefore phase separation will occur.
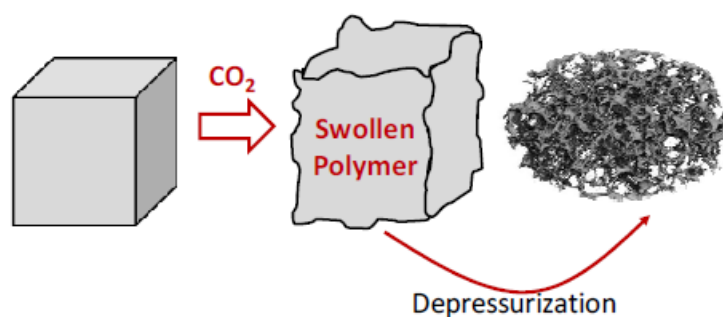
Figure 8: Foaming process schematization. The figure was taken from Temtem[33]

The gas will desorb from the polymer forming pockets of gas inside solid, thus causing physical blowing and the formation of a porous structure. Consequently, to the desorption of CO_2, the plasticization decreases, until the polymer passes to the glassy state, determining the stiffening of the structure.

1.3.2. Emulsion templating

Emulsion templating method allows the preparation of polymers possessing a well-defined porous structure. Firstly, a high internal phase emulsion (HIPE) is formed between two immiscible components, one polar (usually water) and the other non-polar, with the help of an appropriate surfactant. Subsequently the external phase is stabilized, usually by means of a polymerization reaction.

When the internal phase is removed, the product obtained is a replica of the "template" constituted by the emulsion. Because of the fact that the most common internal phases used are oils, the removal step is not easy to accomplish thus assuming fundamental relevance in the determination of the feasibility of the whole process.

The use of $scCO_2$ instead of oils, allows to solve this problem because, under normal conditions of temperature and pressure, CO_2 is a gas. It is sufficient to lower the pressure under P_c to have a gas phase which can be easily vented, leaving a dry product.

Figure 9: Schematization of CO_2/H_2O emulsion templating process. The figure was taken from Temtem[33]

1.3.3. Phase inversion

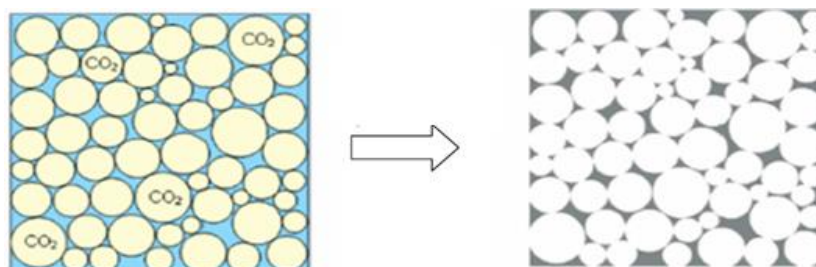Phase inversion process is the most common method for porous membranes preparation. Generally, a polymer solution is distributed homogeneously on a suitable support, which is subsequently immersed in a non-solvent. The solvent/non-solvent exchange causes the precipitation of the polymer, thus the choice of an appropriate solvent/non-solvent system plays a fundamental role on the outcome of the membrane. Other important parameters to control are: concentration of the solution and composition of the casting solution (e.g. use of polymer mixtures, additives), temperature, time of evaporation and humidity.

The phase transition pathway taking place during phase inversion can be represented in a ternary phase diagram as the ones represented in *Figure 10*, where each corner of the triangle represents the pure component (solvent, non-solvent, polymer), while any point inside the diagram represents a mixture of the three components. The diagram is divided into two areas by the binodal curve, which represents the equilibrium boundary between the one phase region, where a homogenous solution can be encountered, and the two-phase region, where the solution separates into polymer-rich and polymer lean phase. The isotherm lines connecting the composition of the two phases formed at equilibrium (polymer lean and polymer rich phases) are called tie-lines.

Depending on the time scale of the non-solvent addition to the system, the composition pathway may or not enter the two-phase region at a certain time, thus yielding different morphology of the membranes[34]. Instantaneous demixing occurs if liquid-liquid demixing starts immediately after immersion and the composition pathway is analogue to the one reported in *Figure 10a*. Delayed demixing occurs if the system is similar to the one reported in *Figure 10b*, where all the compositions directly beneath the top layer remain in the one phase region. In this case the demixing is not started immediately. Anyway after a longer time, also the compositions beneath the top layer will cross the binodal curve, starting the demixing.

Strathmann et al.[35] demonstrated that slow precipitation rates result in a "sponge-like" structure, which allows a low water flux to permeate through the membrane, while fast precipitation rate yields membranes possessing "finger-like" macrovoids, which confer high water permeability properties.

As a general rule, all changes in processing condition that make the precipitation rate slower tend to produce a membrane with sponge-like morphology characterized by low flux, and higher solute rejection if tested in a RO apparatus.

Organic solvents conventionally used for phase inversion are volatile, flammable and should be avoided in a process inspired to the green chemistry principles.

Among the solutions proposed, scCO$_2$ assisted phase inversion is an easy, safe and clean method to produce porous structures. *Kho et al.*[36] where the first ones to report the preparation of membranes exposing a solution of Nylon 6 in 2,2,2-trifluoroethanol to scCO$_2$ to induce phase separation of the polymer solution. Since then many authors have applied this technique and the influence of different parameters such as polymer concentration[37], temperature, pressure[38,39], solvent/non-solvent affinity, depressurization rate[40], foaming process against phase inversion[41], entrainer effect[42] have been evaluated.
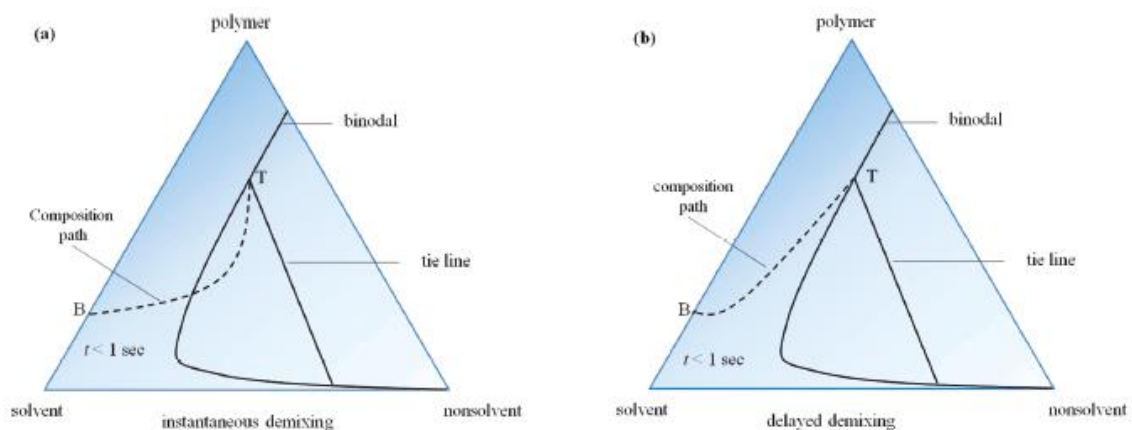

Figure 10: Ternary phase diagrams for a generic mixture of polymer, solvent and non-solvent after a time t <1 sec from the immersion in the non-solvent. (a) instant demixing; (b) delayed demixing.

Besides being a green alternative to organic solvents, $scCO_2$-assisted phase inversion (*Figure 11*) usually happens with the delayed demixing mechanism: in fact when a polymer solution is immersed in a coagulation bath, the external layer of the polymer precipitate rapidly, forming a film that hinders the solvent exchange and thus slows down the process in the core. Given that the precipitation rate deeply influences the outcome of the porous structure of the membrane, the "tuneable" properties of density and viscosity owned by a supercritical fluid constitute a serious advantage compared to organic solvents. As can be noted on the graphic in *Figure 12*, reporting the variation $scCO_2$ density with pressure and temperature, close to the critical point (K_p) the isotherms are almost parallel to the ordinate axis. As a consequence, a small variation in pressure or temperature determines a large change in density. The density is not only closely related to the non-solvent power of CO_2 but also influences the diffusivity, and therefore his precise manipulation is an important advantage in controlling the morphology of the membranes. Many authors[43][44] have analysed the influence of these parameters in $scCO_2$-assisted phase inversion processes and they reported that the average pore size and the porosity decreased by increasing density (higher pressure or lower temperatures). In fact, higher CO_2 density (higher non-solvent strength) determines the formation of a higher number of nucleation points, inducing the formation of small pores in a large quantity. On the contrary, lower
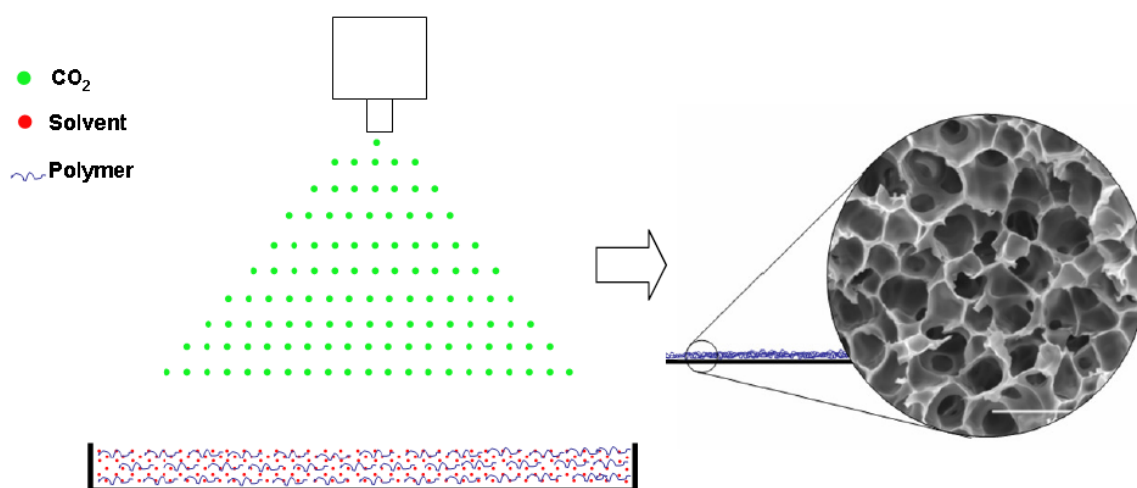
Figure 11: Schematic representation of scCO₂-assisted phase inversion. The figure was taken from Temtem[33]

densities will induce the formation of less nucleation points, thus resulting in a smaller quantity of bigger pores.

As the organic solvent based, also in supercritical-assisted phase inversion technique the initial solution concentration is a key parameter in determining the morphology of the membrane: in general, an increase in concentration determines a decrease in the medium pore size diameter.

Another fundamental parameter to control morphology of the membrane introduced by $scCO_2$-assisted phase inversion is the depressurization time. In particular varying the depressurization time it is possible to modify the top layer of the membrane[36]. In fact, the dense skin layer that forms at the interface between the casting solution and the nonsolvent, acts as a barrier for the diffusion of CO_2 outside the membrane.

Temtem et al. report that for polysulphone membranes, if the pressure is released slowly (1 hour), the nonsolvent diffuses through the top skin layer of the membrane without affecting its surface morphology. On the contrary, a fast release in pressure (1 minute) will originate a stronger driving force for the diffusion of CO_2 outside the membrane, causing some of the pores to blow and therefore explaining the presence of holes in the membrane skin.

Figure 12: Variation of density of scCO₂ with temperature and pressure (left) and Phase diagram of carbon dioxide (right).

1.4. Chitosan and chitin

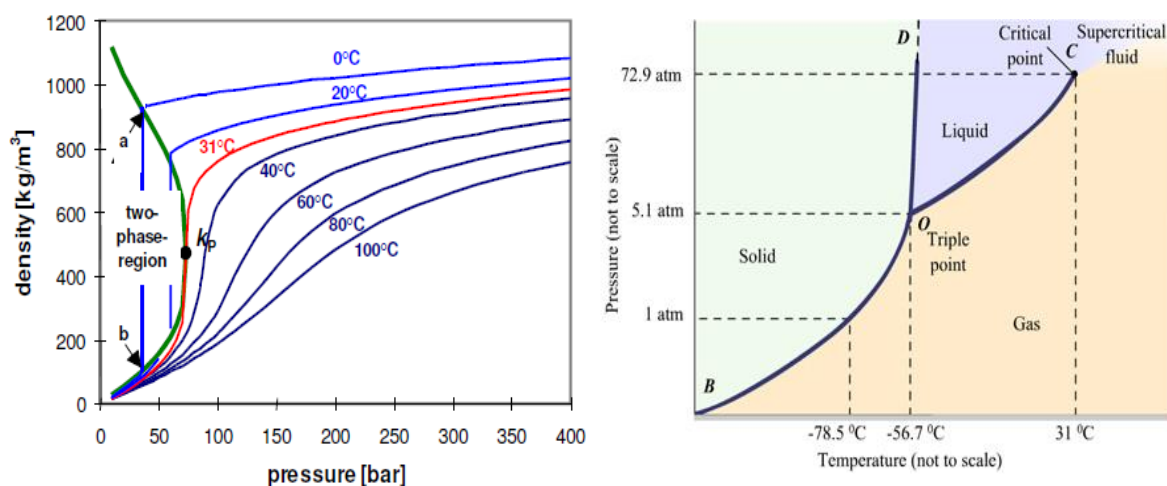Chitosan, whose chemical structure is represented in *Figure 13*, is a poly-amino-saccharide formed by randomly disposed units of D-glucosamine and N-acetyl-D-glucosamine linked β-(1→4). It can be obtained by the deacetylation of chitin, the second most abundant biopolymer in nature after cellulose. Chitin is in fact the main component of the exoskeleton of shellfish such as prawns, crabs and lobsters. However, it can also be encountered in the cell walls of fungi such as *Absidia coerulea* and *Mucor rouxii*.
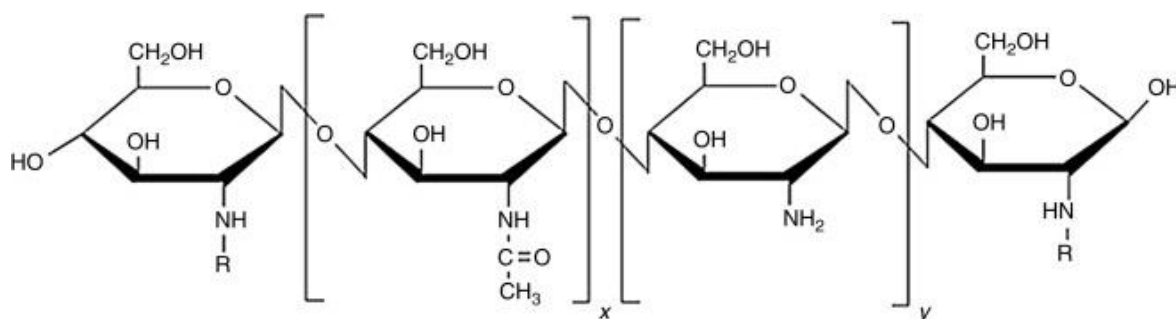
Figure 13: Chemical structure of chitosan

The major part of chitosan is produced from waste streams of the food industry. Shells of shellfish are first dried and subsequently converted into chitin with a transformation involving two main steps: the demineralization process using hydrochloric acid and the removal of proteins, using diluted sodium hydroxide solutions. Given that the process feed is a waste stream and that the proteins and minerals extracted are reusable as fertilizers, it is possible to assess that the aforementioned process has a low environmental impact[45].

Finally, chitosan is produced by chitin deacetylation, carried out by alkaline hydrolysis using concentrated sodium hydroxide and high temperatures or enzymatic catalysis processes. If the deacetylation degree is higher than 50%, the polymer is conventionally called chitosan. Depending on process of deacetylation and the raw material used, chitosan with different deacetylation degree (DD) and molecular weight can be obtained thus resulting in polymers possessing different properties and application fields.

Because of high availability, low price, biocompatibility and biodegradability, chitosan has driven on itself the attention of many researchers and is used in many different fields of application. In fact, possessing a bacteriostatic effect due to his cationic properties[46,47], chitosan increases protective responses in various plants[48,49] and has also been studied for various applications in pharmaceutical industry, either as artificial tissue for wound dressing[50], carrier for drug delivery[51] or excipient[52].

1.4.1. Chitosan in water treatment systems

Many studies demonstrated the suitability of chitosan-based devices in water treatment systems, especially concerning the removal of heavy metal such as $Cr(VI)$[53], $Cd(II)$[54], $U(VI)$[55] from aqueous solution throughout adsorption.

Besides being a green polymer, the main advantage deriving from chitosan use in water purification instead of conventional synthetic material such as styrene-divinylbenzene resins, polyethylene and polyurethane, is the enhancement of the kinetic of sorption. In fact, the presence of polar functional groups in chitosan repeating unit, namely primary and secondary hydroxyl and amino/acetammino groups, confer to the polymer a more hydrophilic behaviour than the aforementioned polymers[14].

The capability of cross-linked chitosan functionalised with NMDG of boron capture has already been studied and resulted very effective. *Sabarudin et al.*[14] have successfully grafted NMDG on the surface of chitosan particles, reporting a maximum adsorption capacity of 22.7 mg/g and a complete removal of boron from a solution with concentration of 100 mg/L after 10 minutes.

The values obtained under the same conditions for the most common commercially available resins used for boron sorption such as Amberlite IRA 743 are much lower (3.1 mg/g[15]), thus making cross-linked chitosan a more suitable material than Amberlite. Nevertheless, the synthesis procedure Sabarudin reported involves protection/deprotection steps of the amino group resulting long, non-eco-sustainable and expensive. Thus the product synthetized is not applicable on a large scale production.

1.5. Boron colorimetric determination

Colorimetry is a spectrophotometric technique used to determine the concentration of coloured compounds in a solution. It may be applied to the quantification of both organic and inorganic compounds, provided that a suitable reagent is chosen in order to react selectively with the analyte, generating a coloured compound called chromophore. The absorbance of the chromophore at a specific wavelength is measured by means of a spectrophotometer and correlated to the concentration in the sample by means of a calibration curve.

Regarding boron determination the most common colorimetric methods are curcumin[56], carmine[57], azomethine-H[58].

For the development of the work reported in this thesis the curcumin method was chosen. This method takes advantage of the reaction represented in *Figure 14,* occurring between curcumin enolate and boric acid in an acidic solution. The reaction yields a red coloured compound called rosocyanine (boron: curcumin 1:2 complex)[59], the driving force leading to his formation derives from the formation of a conjugated system which gives also origin to light absorption. The entire skeleton of curcumin is in resonance with the 1,3-dicarbonil section and the positive charge is delocalized on the entire molecule.

The intensity of the light absorbed by a solution containing rosocyanine is proportional to its concentration, according to Lambert-Beer's law. Usually the analysis is performed at 540 nm because at that wavelength maximum absorbance can be encountered. The sensitivity can be as low as 2 μg/L.
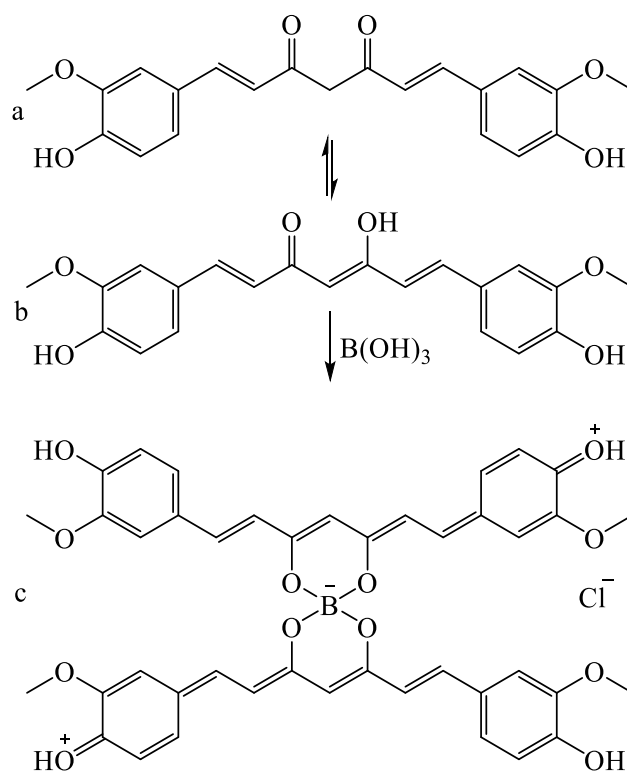
Figure 14: Reaction of boric acid with curcumin to yield rosocyanin; starting from the top curcumine (a), curcumin enolate (b) and rosocyanine (c) are illustrated.

2. Aim of the research

Boron is an element essential for various biological processes, nevertheless at high concentration it can cause health issues in both plants and animals thus making boron a pollutant element. Not only the growing demand for industrial applications (glass, circuits, energy) entails the purification of waste streams, but also solving the problem of drinkable water availability in some areas of the world by desalinization of seawater, which normally holds high boron content, has driven the attention of many researchers towards the production of cost-effective and selective water treatment systems for boron removal.

In fact, boron in aqueous solution is mostly encountered in the form of boric acid whom, being a small molecule is hardly retained by common water treatment systems such as reverse osmosis. Usually reverse osmosis (RO) plants are coupled with a pre-treatment system used to avoid particle, bacterial, colloidal fouling but concerning boron removal, there is no pre-treatment system sufficiently effective.

The aim of this work is to produce and characterize low cost and effective polymeric adsorbents capable of removing boron in aqueous solution at neutral pH, taking advantage of the interaction reaction occurring between boric acid and alcoholic groups, which are able to form specific complexes and therefore confer to the adsorbent selectivity towards boron. In order to be implemented in a RO pre-treatment system, the adsorbent was designer to be reusable after regeneration and to allow the recovery of boric acid in order to valorise the waste stream and increase overall process sustainability.

With the purpose of achieving this goal two different kind of devices were designed, produced and tested.

Chitosan hydrogel beads were produced and subsequently functionalized with N-methyl-D-glucamine. NMDG is an amino sugar able to form stable complexes with boric acid at neutral pH with an enhanced kinetic if compared to other polyols. However, in contact with an acid solution, boric acid dissociates from the complex and the device can undergo regeneration and thus be reutilized. After confirming that the grafting with NMDG was successful, the adsorption capacity was tested in order to compare the material with other adsorbents reported in literature or commercially available.

However, the most consistent part of this thesis involves the production of PVA/chitosan membranes, which was carried out taking advantage of $scCO_2$-assisted phase inversion technique. The use of supercritical carbon dioxide in polymer processing is an innovative and versatile approach. The versatility derives from the numerous parameters that allow controlling the morphology of the processed polymer compared to a traditional phase inversion process and the possibility to obtain dry and ready-to-use membranes. In addition, CO_2 is non-toxic and environmental-friendly.

The investigation was focused on the production and characterization of membranes with different porosity. Following the functionalization reaction previously tested with the beads and the confirmation of the grafting of NMDG on membrane surface, the permeability, the adsorption capability and regeneration behaviour were investigated in order to evaluate if the device produced fits the requirements for the application in microfiltration.

The work was carried out in the laboratories of LAQV-REQUIMTE, FCT of Universidade NOVA de Lisboa. LAQV is an acronym for Laboratório Associado para a Química Verde and therefore particular attention was paid in the eco-sustainability of process and products, choosing when possible reagents and solvents with lower environmental impact and possibly coming from waste streams of the industries or renewable resources.

3. Experimental

3.1. Materials and instruments

Chitosan (Mw = 190,000-310,000, 75-85% deacetylated), epichlorohydrin (ECH), poly-vinyl alcohol (PVA, Mw = 89,000-98,000 99+% hydrolized), dioxane, 2-propanol, 2-ethyl-1,3-exanediol were purchased from Sigma Aldrich. Anhydrous absolute ethanol and chloroform were purchased by Carlo Erba Reagents (Italy), concentrated sulphuric acid (95-97% purity) and glacial acetic acid (purity ≥ 99%) were purchased from Honeywell, methyl-ethyl-ketone (purity 99% min) was purchased from May & Baker. Sodium hydroxide pellets were purchased from Alpha Aesar and boric acid was purchased from AppliChem (Germany). CO_2 and Argon were purchased from Air Liquide (Portugal). Aqueous solutions were prepared using Milli-Q water (19-17 μΩ). All the reagents were used as received without further purification.

ATR spectroscopy was registered using a PerkinElmer Spectrum Two instrument in the 4000–400 cm^{-1} region with a resolution of 2 cm^{-1}. The spectres were obtained by the sum of 20 scans.

Optical microscopy images were recorded with a Morphology G3 instrument, while scanning electron microscopy (SEM) images were recorded with a Hitachi S-2400 instrument, with an accelerating voltage set of 15kV.

Absorbance at 560 nm was measured with an Infinite 200 microplate reader, using the Tecan i-control software. The bandwidth was 10 nm and the number of flashes was set at 25.

3.2. Beads preparation and characterisation

3.2.1. Preparation of chitosan beads (CB)

The chitosan beads (CB) were prepared using a Nisco VAR J1 co-axial air bead generator instrument (*Figure 15*), consisting of a syringe pump injecting the polymer solution into a small needle. On a parallel direction is directed an air flow, which pulls droplets from the needle tip into a gelling bath, typically a solution of NaOH 3.75 M. Therefore, the beads are formed with a smaller diameter than the ones obtained by gravity driven dropping.

The beads were prepared using a 2% wt. of chitosan in 2% v/v acetic acid solution, with an air flow of 2.85-2.95 L/min and the flow of polymer solution was set at 5 ml/h.

The beads were left hardening in the precipitation solution agitated through an orbital shaker at 100 rpm for 24h at room temperature. Subsequently CB were washed with Milli-Q water until neutrality was obtained.
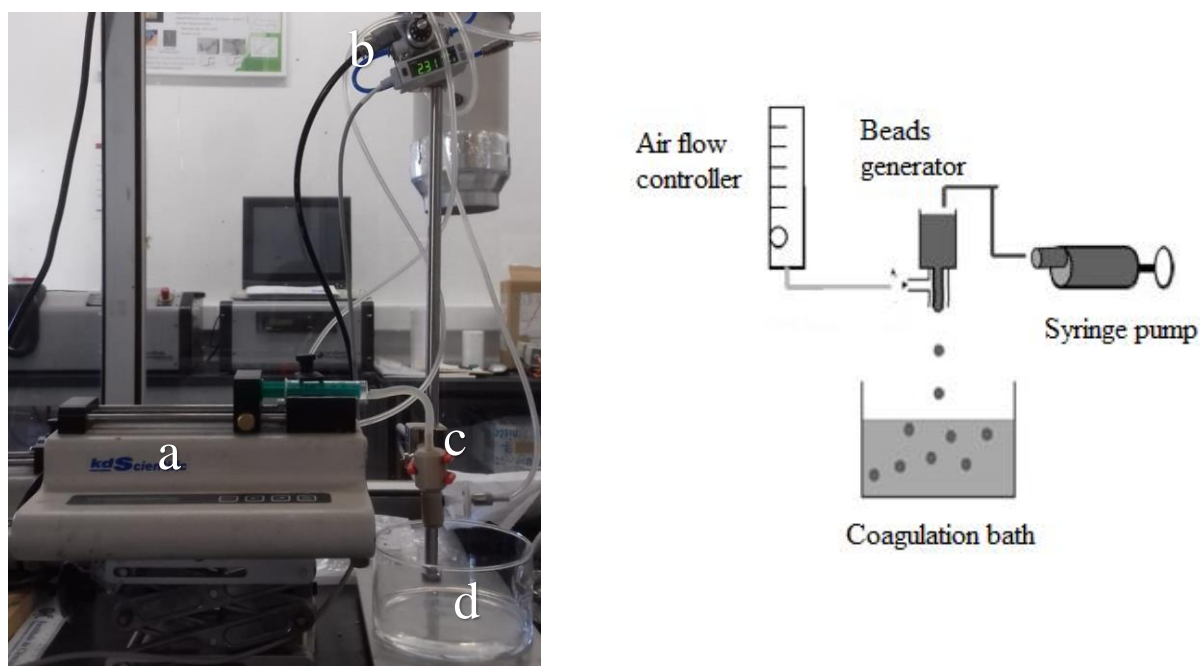

Figure 15: Set-up used for beads generation (left); a) syringe pump; b) air flow controller; c) beads generator; d) precipitation bath. On the right is reported a schematic figure of the apparatus.

3.2.2. Preparation of cross-linked chitosan beads (CCB)

1.5 g of CB were suspended in a glass flask containing 15 ml of H_2O and 25 ml of i-PrOH. The pH was adjusted to 10 by adding a solution of NaOH 0.8M. Finally, 6 ml of epichlorhydrine (ECH) were added.

The suspension was heated at 60°C for 4 hours in a thermostatic orbital shaker. The stirring speed was set at 100 rpm.

The cross-linked beads (CCB) were rinsed two times with EtOH to remove unreacted epichlorhydrine and four times with Milli-Q water, to remove EtOH..

3.2.3. Preparation of NMDG-grafted cross-linked chitosan beads (CCBMG)

In a glass flask containing 7.5 ml of NaOH 0,8M solution and 25 ml of dioxane, 0.3 grams of NMDG were dissolved. Subsequently 1.5 g of CCB was transferred in the flask.

The flask was stirred on a thermostatic orbital shaker at 100 rpm, heating at 60°C for 3 hours.

The resulting functionalised beads (CCBMG) were washed two times with ethanol and four times with Milli-Q water, in order to remove unreacted NMDG.

3.2.4. Adsorption isotherms and regeneration behaviour

0.1 g of CCBMG were transferred in a vial and suspended in 10 ml boric acid solution with a concentration ranging from 50 to 2000 mg/L. Vials containing the aforementioned suspension were agitated at 150 rpm in a thermostatic orbital shaker at 30 °C for 24 hours. The liquid was

separated from the solid particles by settling and the solutions were then filtered using a syringe filter with pore diameter of 0.2 µm and stored in a 5 ml plastic tube.

The beads regeneration behaviour was tested in Supelclean ^{TM} LC-Ph SPE 3 ml columns for liquid phase extraction. 1 ml of beads (weight 0.6 g) was transferred in the column between two porous discs. 2 ml of Milli-Q water were then added and the water was left flowing slowly overnight without applying any pressure in order to homogeneously pack and condition the column.

Subsequently 2 ml of boric acid solution at a concentration of 100 mg/L were fluxed applying a slight vacuum with a Supelco VISIPREP^{TM} instrument. The solution was then collected in a clean plastic tube.

The regeneration was effectuated by fluxing 10 ml of 0.5 M HCl solution in order to desorb boric acid. Then Milli-Q water was loaded in the column and fluxed until neutrality of the permeate was obtained. The procedure was repeated for three times.

3.3. Membrane preparation and characterisation

3.3.1. Preparation of the membranes

The chitosan-PVA membranes were prepared using the scCO$_2$-assisted phase inversion method using a high pressure apparatus described in *Figure 16*. The fundamental unity of the apparatus, where phase inversion occurs is a stainless steel cell specifically designed which is described in detail by *Temtem et al.*[39].

The stainless steel lid of the cell contains holes for the inlet valves of CO$_2$. Entering from the top, the fluid flows through a Rashig rings bed sustained by a porous metallic disc apt to favour the omogeneous distribution of CO$_2$ on top of the casting solution surface. The casting solution is situated in the bottom part of the cell, supported by a stainless steel plate. CO$_2$ flows from

the top, gets in contact with the surface of the solution and exits the cell throughout four holes placed just above the level of the stainless steel plate. The sealing between lid and pan of the cell is granted by a teflon O-ring.

The cell is immersed in a bath of transparent glass allowing visual inspection, thermostated by means of a Hart Scientific Model 2200 controller that maintains the set temperature within a range of ±0.01 °C. The pressure is monitored using a pressure transducer (Setra Systems Inc., Model 204) with a precision of ± 100 Pa and it is regulated by a back-pressure regulator Jasco 880-81, which also allows to separate CO_2 from the ethanol/water mixture.

In all the experiments a casting solution with a concentration of 17% wt. was prepared dissolving (90°C, 1hour) PVA/chitosan in a ratio 87/13 in 2% vol. acetic acid. A weighted amount of the viscous solution was homogeneously distributed on the stainless steel plate and placed inside the cell. The excess of solution was then eliminated levelling with a spatula at the
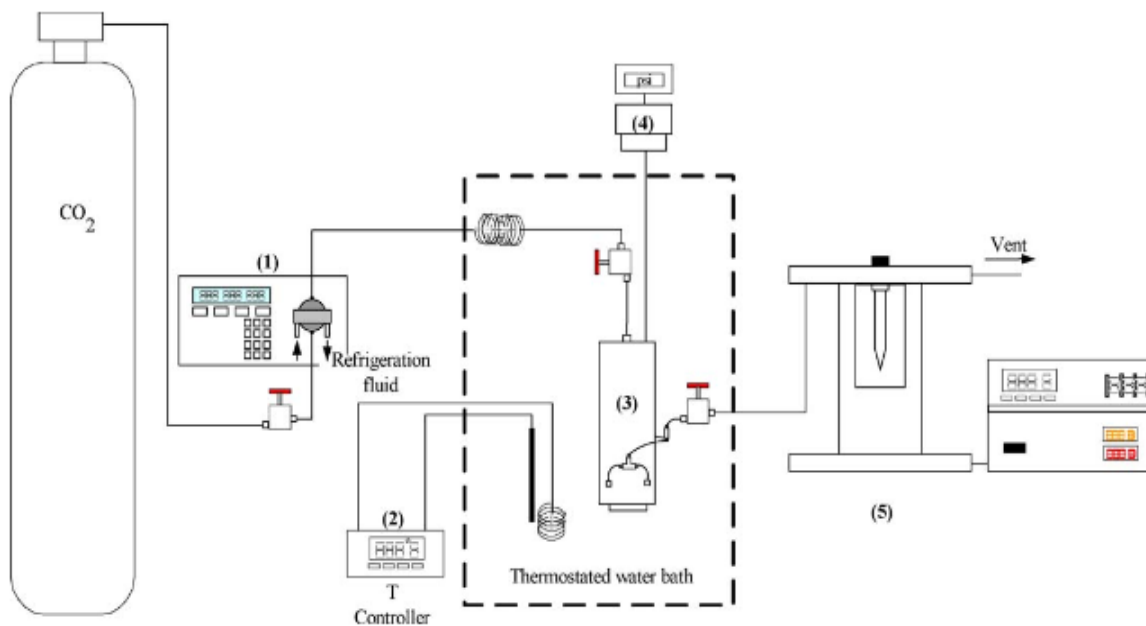

Figure 16: Layout of the high pressure apparatus for membrane formation. (1) Knauer 40P piston pump; (2) temperature controller; (3) high pressure cell; (4) pressure indicator; (5) back pressure regulator. The figure was taken from Temtem[33]

level of the weir of the plate. Subsequently the cell was immersed in the thermostatic bath at 45°C and CO_2 was added at a flow of 4.5 ml/min in order to pressurize the cell at 200 Bar.

After reaching the operative pressure, the ethanol flux was started at 0.5 ml/min and the non-solvent mixture, which is therefore composed by CO_2 and ethanol in a 9:1 ratio was let flow in the cell for 2 hours. The use of a second component in the non-solvent, is necessary to increase water miscibility with $scCO_2$ and cause the phase separation. Subsequently, a flow of 10 ml/min of pure CO_2 was passed in the cell during 40 minutes in order to remove all the ethanol. At the end of the washing, the system was depressurized in a time lapse of 10 or 15 minutes. The cell was carefully opened after reaching room temperature and the membrane was removed from the support.

3.3.2. Functionalization of the membranes

In the first step of the reaction, an H_2O/*iso*-propanol 6:10 mixture was prepared in a graduated glass cylinder and its pH was adjusted to 10 using a solution 0.8M of NaOH. 20 ml of the aforementioned solution were transferred into a glass reactor. Subsequently the membrane was immersed in the liquid and finally 3 ml of ECH were added. The reactor was closed with a lid and put into a thermostated orbital shaker. The temperature was set at 40 °C and the orbital shaking at 150 rpm. The reaction was carried out for 4 hours.

At the end of the reaction the membranes were separated from the liquid and rinsed two times with fresh Milli-Q water, and then suspended in Milli-Q water agitating by means of an orbital shaker at room temperature and 150 rpm for a total time of 20 minutes.

For the second step of the reaction, consisting of functionalization with NMDG, a NaOH 0.8M/dioxane 3:10 mixture was prepared in a graduated cylinder. 20 ml of the aforementioned solution were transferred into a glass reactor. 0.3 grams of NMDG were weighted and dissolved in the solution. Finally, the membrane was immersed in the solution and the reaction was carried out for 3 hours at 30 °C in a thermostated orbital shaker with shaking speed set at 150 rpm.

After the reaction, the membranes were separated from the solution, rinsed with fresh water, and then left agitating in a glass vessel containing 50 ml of water inserted in the shaker for 10 minutes at 150 rpm and room temperature.

The membranes were then dried at room temperature between two sheets of filter paper. During the drying process a weight was applied above the membranes to prevent loss of the flat shape.

3.3.3. Permeability measurement of the membranes

The permeability of the membranes to pure water was determined by measuring the distilled water flux through them using the 10 ml filtration stainless steel high-pressure cell with an internal diameter of 2 cm illustrated in Figure 17.

The membrane was cut into a disc of the dimensions required to fit the cell and carefully placed on top of a support containing channels that allow permeate to flow outside of the cell throughout a silicon tube. A Teflon O-ring was placed on top of the membrane to ensure the sealing and the support was inserted in the cell from the bottom and fastened with the bottom lid. 10 ml of Milli-Q water were then transferred in the cell from the top. Finally, the top lid was closed and a pressure varying from 0 to 8 bar was applied using compressed Argon. Measured volumes of liquid were collected in a graduated cylinder or in a 1.5 ml eppendorf tubes depending on the flow rate and time was measured.

The permeability value was obtained by the slope of the linear relation between flux and pressure according to the Darcy law:

$$F = L_p \times \Delta P$$

Where:

F is the flux ($Lm^{-2}h^{-1}$)

L_p is the permeability ($Lm^{-2}h^{-1}MPa^{-1}$)

ΔP is the pressure drop on the two sides of the membrane (MPa)

3.3.4. Adsorption dynamic test and regeneration test of the membranes

The sorption dynamic test on membranes was effectuated using the 10 ml filtration stainless steel high-pressure cell with an internal diameter of 2 cm illustrated in Figure 17.

The membrane was cut into a disc of the dimensions required to fit the cell and carefully placed on top of a support containing channels that allow permeate to flow outside of the cell throughout a silicon tube. A Teflon O-ring was then placed on top of the membrane to ensure the sealing and the support was inserted in the cell from the bottom and fastened with the bottom lid. 5 ml of 50 mg/L boric acid solution was then transferred in the cell and the top lid was closed. Pressure was applied by compressed argon gas in order to flow the solution. The permeate was collected and fluxed for a second time. After the second filtration the volume of the final permeate was measured in a graduated cylinder and the liquid was then stored in a Falcon tube.

Subsequently the membranes were regenerated by immersion in 10 ml of solution 0.5 M of HCl, agitated for 2 hours in an orbital shaker at room temperature and washed with Milli-Q water until neutrality was obtained.

The filtration/regeneration cycle was repeated for three times.

Figure 17: Stainess steel filtration unit used for flux measurements and adsorption dynamic test. a) top lid; b) bottom lid; c) gas inlet pipe; d) permeate outlet pipe; e) solution tank.

3.4. Boric acid quantitative analysis with curcumin method

For boron determination by the curcumin method, the protocol proposed by *Mohan et al* [60] was applied.

A mother solution of boric acid was prepared in a volumetric flask by dissolving 0.5000 ±0.0005 g of boric acid in 500 ml of Milli-Q water. The solution was transferred in a plastic vessel in order to avoid solubilisation of the boric acid contained in the glass.

The extraction solution was prepared dissolving 2-ethyl-1,3-hexanediol 10% in chloroform in a 5 ml plastic tube.

The acid mixture was prepared mixing concentrated sulphuric acid and glacial acetic acid in 1:1 ratio in a 10 ml plastic tube.

The curcumin solution was prepared dissolving curcumin in methyl-isobutyl-ketone at a concentration of 2 mg/ml in a 5 ml plastic tube.

New solutions were prepared and used for each analysis, and a maximum of 24 samples were analysed daily in order to minimize the differences in reaction time between the samples.

Standards for the calibration curve with a concentration of 0.02; 0.05; 0.1; 0.2; 0.4; 0.8 mg/L were prepared by successive dilution of the mother solution. For the blank Milli-Q water was used. All the samples were diluted to fit in the concentration range of the calibration curve.

300 µl of each sample (including the blank and the standards), were transferred into 1.5 ml plastic tubes. The samples were acidified by adding in the tube 100 µl of 0.1 M HCl. Subsequently the samples were mixed by vortex and incubated for five minutes at room temperature.

70 µl of extraction solution was then added and each tube was mixed by vortexing for 30 seconds. After 5 minutes the vortex mixing was repeated for another 30 seconds. The tubes containing the samples were then centrifuged at 15000 x g speed for 5 minutes in order to have a clear phase separation of the organic phase.

200 µl of acid mixture were transferred into new 1.5 ml plastic tubes. The acid mixture is a very viscous solution and in order to have more accurate samples the plastic micropipette tip was cut in order to have a bigger tip diameter.

50 ml of the lower organic phase obtained after centrifugation were added to the new tubes (*Figure 18*, picture A). This operation needs to be done quickly because leaking of chloroform out from the micropipette tip can cause pipetting errors. Subsequently the tubes were mixed by vortex.

250 µl of curcumin solution were added and the tubes were shaken well until a homogenous dark purple colour was observed (*Figure 18*, picture B). The tubes were centrifuged at a speed of 15000 x g for 1 minute in order to remove the liquid from the wall and then incubated at room temperature for 1 hour. After this time, the reaction was stopped by adding 500 µl of Milli-Q water and the tubes were mixed gently by inverting them.

Another centrifugation at 15000 x g was effectuated for 1 minute in order to cause phase separation. The absorbance of each well of an empty 96-well UV microplate was recorded and then 200 µl of the upper organic phase (*Figure 18*, picture C) were transferred into microplate and the absorbance at 560 nm was measured.

The last step was executed for a maximum of 8 samples per time in order to avoid sample volatilization, which may affect data reliability. Thermo Scientific MATRIX® polypropylene microplates were used for the analysis in order to avoid solubilisation of polystyrene contained in common microplates. The absorbance value of the samples was calculated subtracting the absorbance of the empty microplate from the one of the wells containing the sample. The concentration was calculated from the calibration curve.
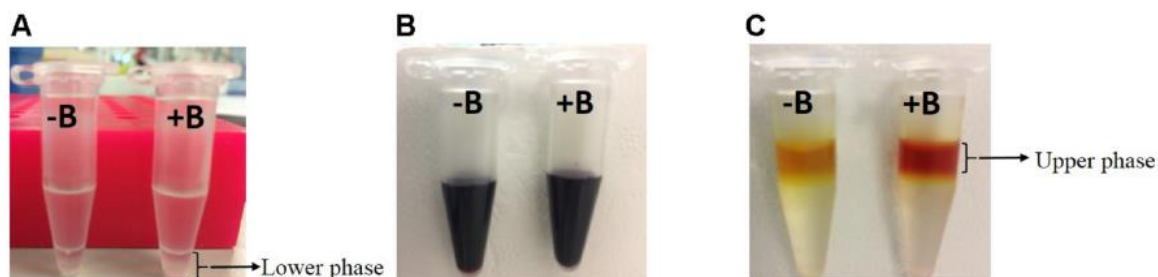

Figure 18: Steps showing phase separation and colour development in the absence (-B) or presence (+B) of boron

4. Results and discussion

4.1. Beads preparation and characterization

The beads were prepared using a Nisco VAR J1 air beads generator instrument. A preliminary scanning test of solutions at different concentrations was necessary in order to determine the solution with the optimal viscosity (*Table 3*).

Table 3: Concentration values of the solution tested and particle shape.

Concentration (% wt/V)	Particles shape
1.2	not formed
1.5	platelets
2.0	beads
2.5	beads
3.0	none

In fact, at low concentration the viscosity of the solution is too low and the cohesion forces of the droplet are not strong enough to resist the impact with the surface of the precipitation solution. Thus, for concentrations equal or lower than 1.5% either no particle formation can be observed or the jellification freezes the structure of the droplet in a platelet shape, which is not suitable for the final application in a packed column.

By using solutions at higher concentration, it is possible to obtain regular and spherical beads. Nevertheless, it was observed for a 2.5% concentration that after few droplets the pipe connecting the syringe to the needle disconnected due to the obstruction of the needle. The solution was too viscous to flow smoothly and thus pressure increased too much in the system. In order to prevent pressure increase it was necessary to decrease the flux slowing down the syringe pump to 1 ml/h, thus allowing stress relaxation in the needle. The solution 3.0% hinders the flux through the needle also at low speed of the pump.

A compromise between the experimental time required for the formation of a large quantity of beads and the quantity of polymer contained in each bead is therefore needed, for this reason the solution chosen to carry out the following work had a concentration of 2.0%.

In order to graft NMDG to the polymeric chains of the beads, a reaction pathway proposed by *Quiang et al.*[61] was used. It consists of two steps illustrated in *Figure 19*: the functionalization of chitosan beads (CB) with ECH, which yields cross-linked chitosan beads (CCB) possessing epoxy functionalities, and the further reaction of the remaining epoxy group with NMDG, which yields NMDG-functionalized cross-linked chitosan beads (CCBMG).

The first step consists of a nucleophilic substitution to the ECH molecule. The nucleophile may be either the secondary amine or the hydroxyl groups of chitosan, while the leaving group may be either the Cl atom or the oxygen forming the epoxy group. As shown in *Figure 20* the nucleophilic attack on the epoxy group leads to the formation of an intermediate, which can evolve following two different pathways:

a) An intramolecular reaction between the nucleophile hydroxylate and the chlorine atom acting as a leaving group, which leads to the formation of a new epoxy functionality;

b) An intermolecular reaction between the nucleophile hydroxylate and either an epoxy ring bounded to the polymer chain or a molecule of ECH, causing the formation of a ramification containing the epoxy group or an intermediate which in turn can evolve again throughout reaction pathways *a* or *b*.

The possibility to react with other ECH molecules may lead to polymerization reaction causing the formation of ramifications and/or crosslinking. Consequently, given the increase of molecular weight, CCB cannot be anymore solubilized, while CB can be easily dissolved in acidic water.

Due to the variety and abundance of reactive sites in chitosan macromolecule and the large excess of ECH in the reaction medium, the possible combinations of CCB structures are countless. *Figure 19* evidences one of the possible products, where both the epoxy groups and the crosslinking are present.
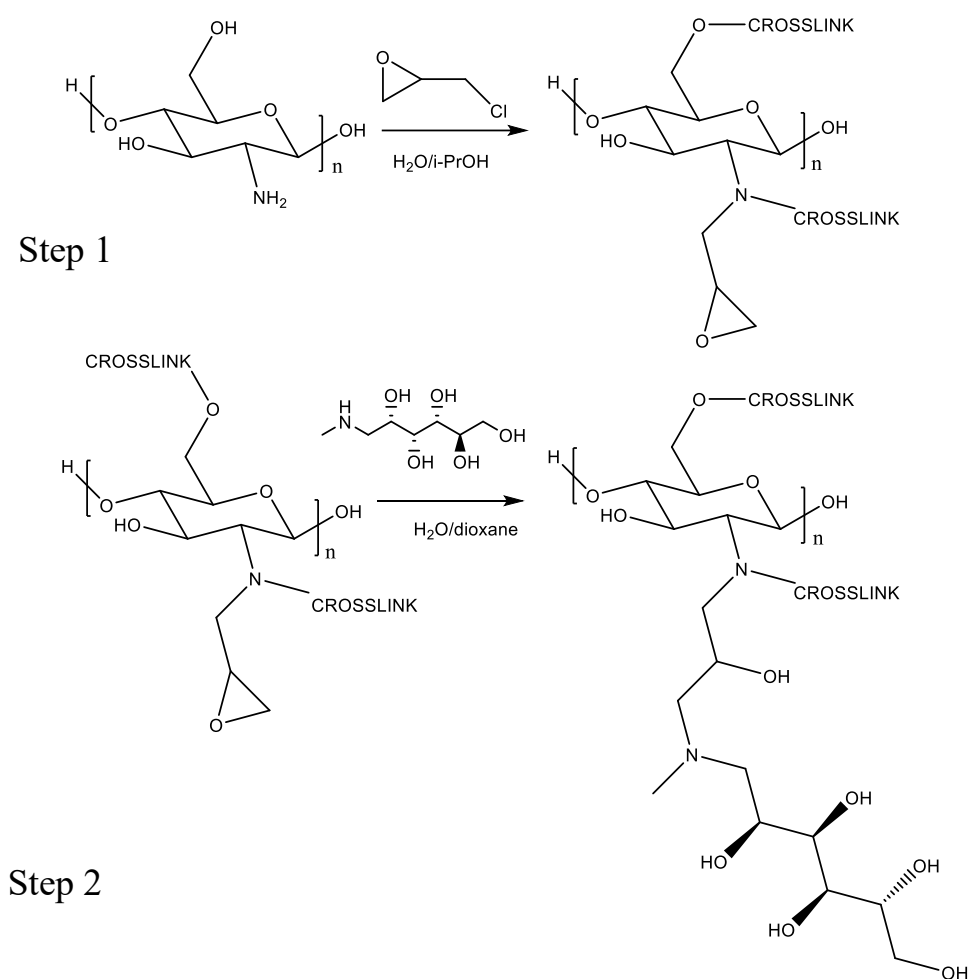

Figure 19: Reaction scheme for the functionalization of the beads: ECH crosslinking (top) and NMDG functionalization (bottom).
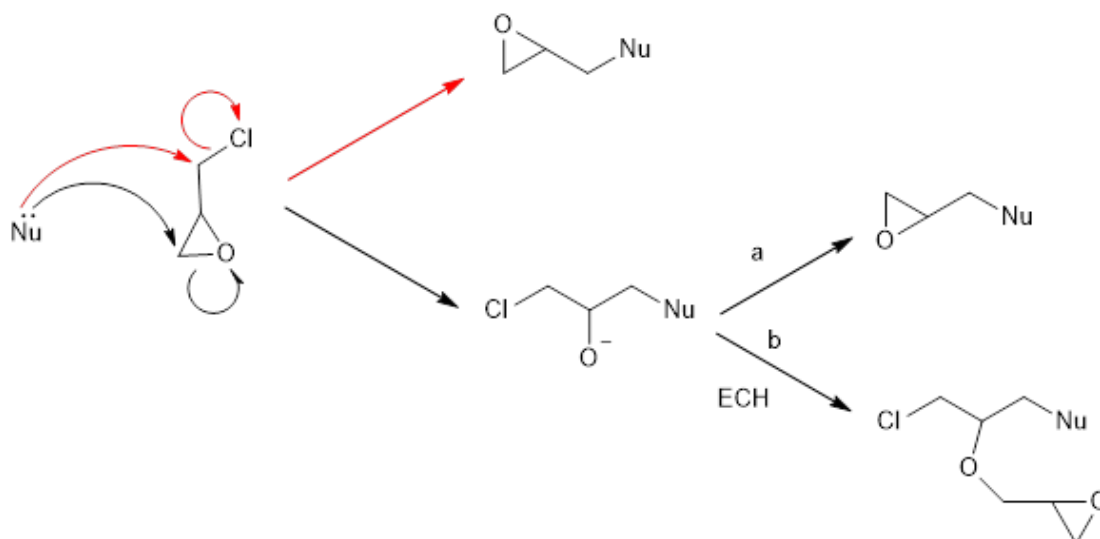
Figure 20: Detail of possible reaction pathways for step 1.

The epoxy groups that did not react in step 1 represent the reactive site for the grafting of the NMDG moieties. The grafting reaction is again a nucleophilic addition, which causes the epoxy ring opening. The nucleophile is the amino group of NMDG, which must be added in excess in order to limit further crosslinking.

Reactions reported in literature[63] used a large excess of the amino sugar (NMDG/chitosan 12:1 wt. /wt.) which is not acceptable in a green chemistry inspired reaction. Thus, in the work presented in this thesis the NMDG/chitosan ratio was drastically diminished to 0.2 wt./wt., corresponding to a ratio 1:1 in moles in the limiting case that during the first step no crosslinking occurred and all the reactive sites have been functionalized with ECH. This means that even adding 60 times less NMDG than the quantity reported in literature, it was possible to have an excess of reagent.

The resulting beads were observed by optical microscopy and the photographs are shown in *Figure 21*. The diameter of the beads varies from 400 to 800 µm, and the shape is approximately spherical.
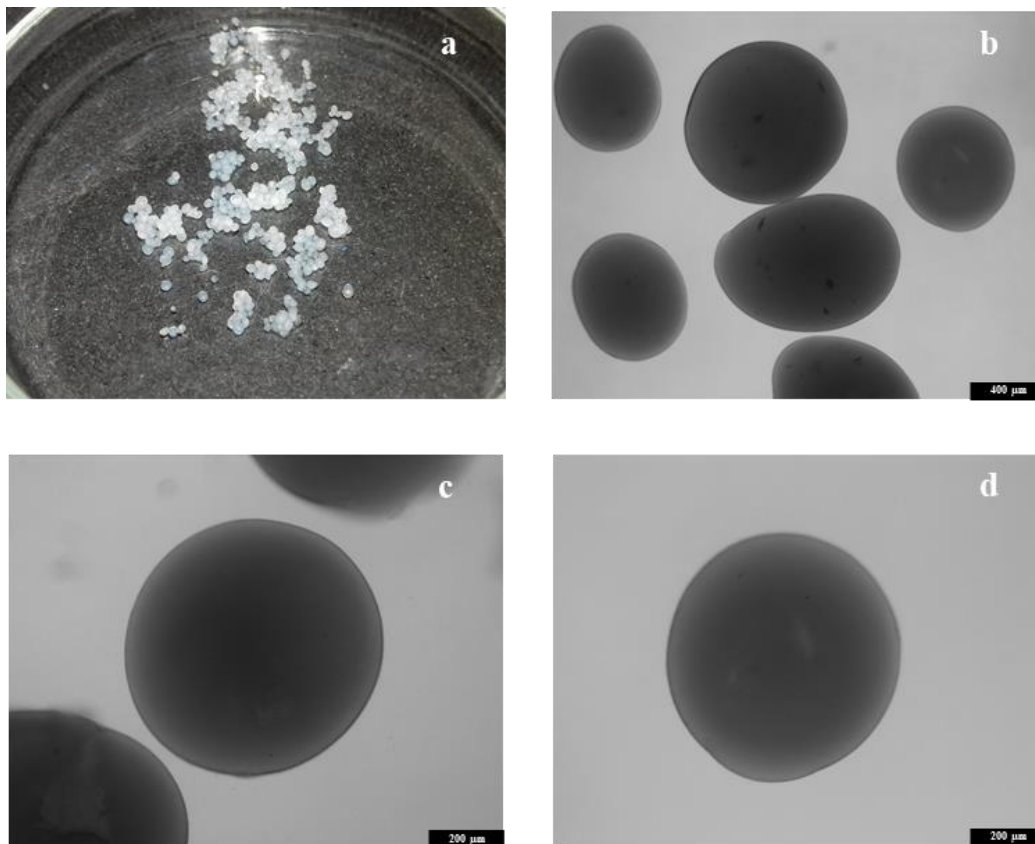
Figure 21: Optical microscopy images of the beads. a) natural dimensions CCBMG; b) CCBMG 25X; c) CCBMG 50X; d) CB 50X.

From the optical micrographs, no substantial difference can be noted between CCBMG (c) and CB (d) therefore the functionalization reactions, which involve suspending the beads in different solvent mixtures, do not affect the morphology and no shrinking or swelling is observed.

Considering that the beads are insoluble, in order to confirm the grafting of both ECH and NMDG onto chitosan chains, it was impossible to use commonly adopted techniques such as nuclear magnetic resonance, therefore an ATR spectrum of the solid was recorded.

The plot in *Figure 22* reports the data obtained from ATR analysis for CB, CCB, and CCBMG. The peak at 1648 cm^{-1} is related to the amidic bond due to the acetyl group of the N-acetyl-D-glucosamine units (chitosan used possess a deacetylation degree between 75 and 85%). This peak does not shift after functionalization, suggesting that the acetylated nitrogen atoms do not

react. The peak at 1590 cm^{-1} in CB spectra is due to the bending vibration of N-H bond of the amine. It can be observed in the spectrum of CCB that this shifts to 1570 cm^{-1} due to the grafting of ECH. Given that the signal attributed to N-H bonds does not completely disappear, it can be assessed that only one ECH unit is added to the amino functionality, probably due to steric hindrance. Another remarkable peak present only in CCB spectrum can be found at 800 cm^{-1} and may be attributed to the absorption of the epoxy ring, meaning that ECH has been grafted.

Comparing the spectrum of CCB with the one of CCBMG two variations can be observed: the disappearing of the peaks at 800 cm^{-1}, and 740 cm^{-1} indicating that the epoxy rings have reacted and the appearance of a new peak at 1463 cm^{-1} due to the C-H bending vibration of the methyl group bound to the nitrogen atom of glucamine moiety, which confirms the grafting of NMDG on chitosan chains.
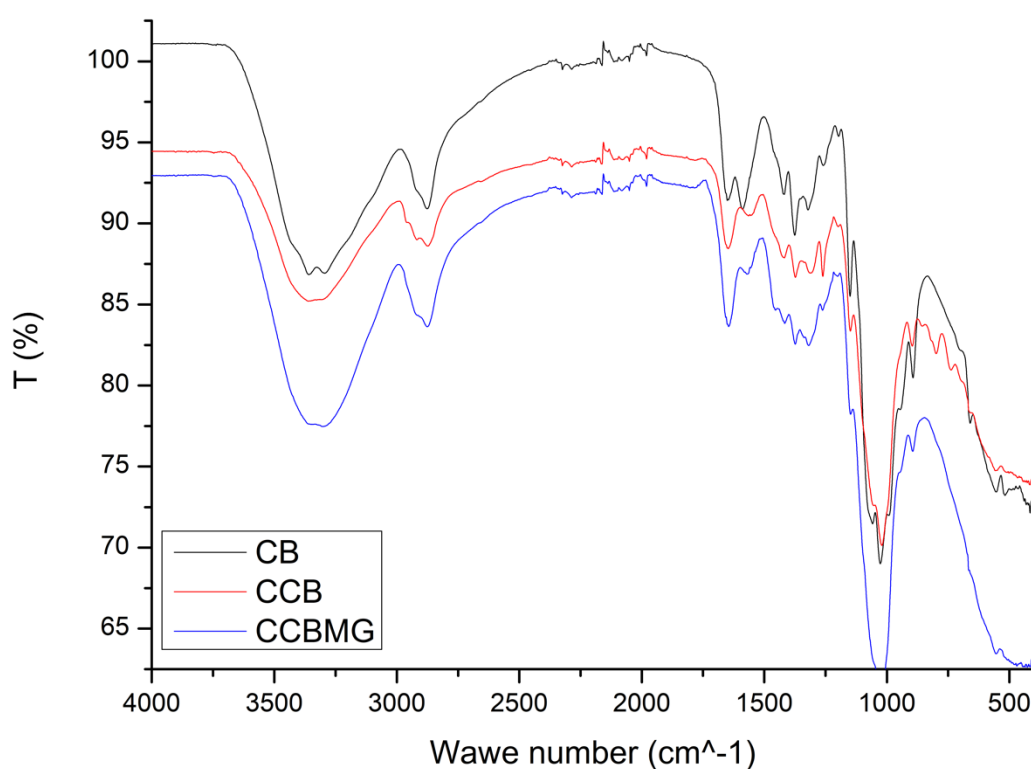

Figure 22: ATR spectra of CB (black) CCB (red) and CCBMG (blue).

4.2. Adsorption studies and regeneration behaviour of the beads

The influence of boric acid solution concentration on the adsorption capability of CCB and CCBMG at the equilibrium was evaluated by suspending a known mass of beads in solutions containing boric acid at different concentrations. After the time of experiment, the solution was separated in order to execute a quantitative analysis of boric acid concentration.

The concentration on the adsorbent was then calculated by a simple mass balance *(Equation 3)*:

$$q_e = (C_0 - C_e) \times V/M \quad (3)$$

Where:

q_e is the equilibrium concentration on the adsorbent (mg/g)

C_0 is the initial concentration of the adsorbate, which is the molecule undergoing adsorption, in the aqueous solution (mg/L)

C_e is the equilibrium concentration of the adsorbate, in the aqueous solution (mg/L)

V is the volume of aqueous solution (L)

M is the mass of adsorbent used (g)

From the plot in *Figure 23,* reporting the concentration on the beads surface versus the concentration in the solution at equilibrium, it can be observed a remarkable difference between the plots of CCB and CCBMG. In fact, q_e does not grow with the solution concentration for CCB because the adsorption capability of the beads without NMDG moieties is limited by the mechanism of physical adsorption.

This is not true for CCBMG that are able to absorb more boric acid as the equilibrium concentration of the adsorbate increase, suggesting that the surface of the functionalized beads possess an improved affinity for boric acid and borate ion if compared with CCB. No multilayer formation is observed in the investigated range of concentration.

Data obtained from batch adsorption experiment was elaborated using the Langmuir adsorption model, which describes the equilibrium distribution of the adsorbate between the adsorbent and the solution. This model is suitable to describe both chemisorption and physical adsorption. It assumes that the adsorbate interacts with the adsorbent surface by forming a monolayer.
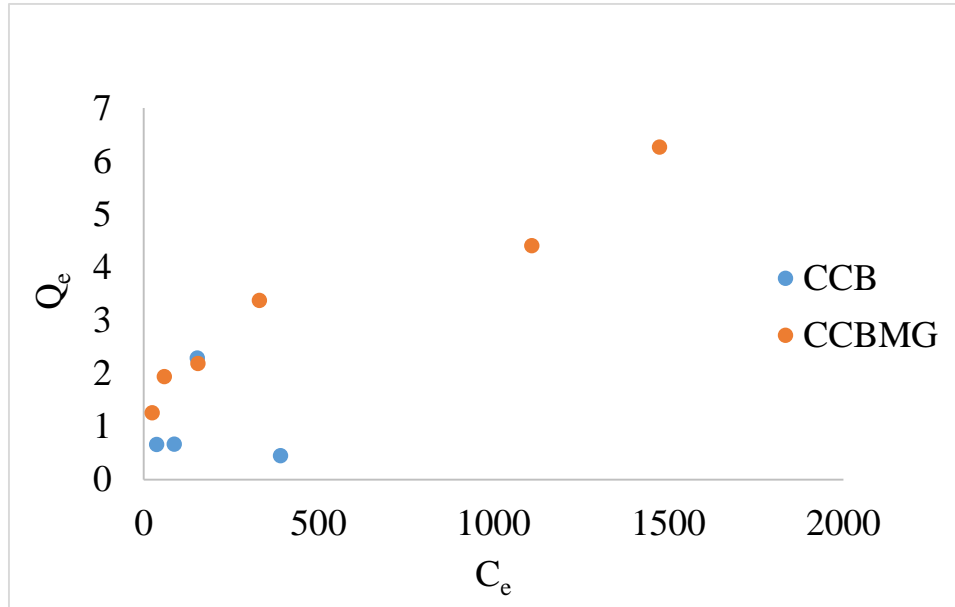
Figure 23: Surface concentration on the adsorbent (q_e) obtained by changes in the equilibrium concentration (C_e).

Equation 4 is the linearized Langmuir equation, which was used to fit the experimental data both for CCB and CCBMG. The graphics obtained are reported in *Figure 24*.

$$\frac{C_e}{q_e} = \frac{1}{Q^0 b} + \frac{1}{Q^0} C_e \quad (4)$$

Where:

Q^0 is the monolayer adsorption capacity (mg/g);

b is a constant related to the free energy of adsorption and the reciprocal of the concentration at which half of the adsorption sites are saturated.

The values of Q^0 calculated from *Equation 4* are 6.2 mg/g and 0.43 mg/g for CCBMG and CCB respectively. The increasing of the adsorption capacity of the monolayer after the addition of NMDG confirms that the grafting reaction has been successful.

Figure 10: Linearized Langmuir fitting for CCBMG (left) and CCB (right).

Q^0 is recognized as an efficient parameter for the evaluation of adsorption capability and it is therefore used to compare different adsorb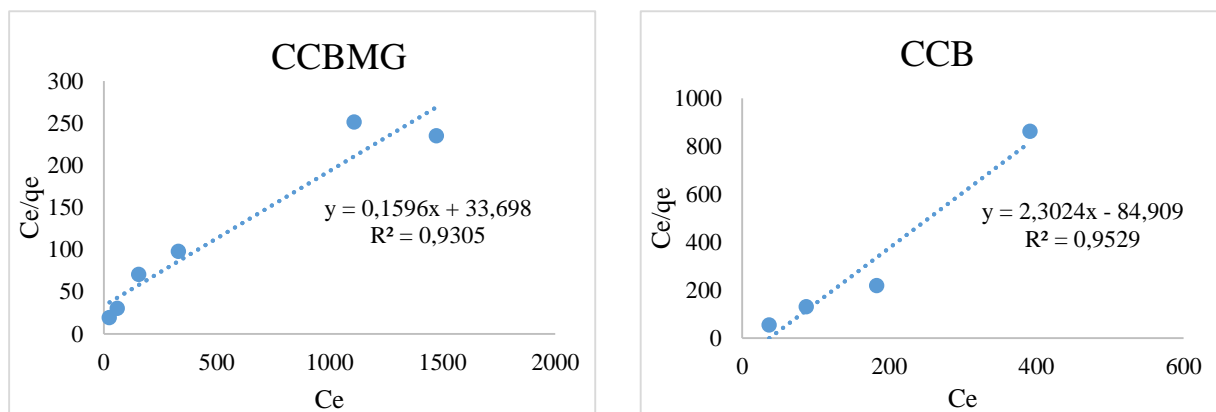ents. In *Table 4* are represented the values of monolayer capacity Q^0 of different adsorbents containing NMDG reported in literature. Comparing CCBMG beads with the other chitosan-based adsorbent it is possible to notice that the product presented in this work possess a smaller capacity for boron removal. Nevertheless, it must be pointed out that, as was previously discussed in Section 1.2.1. the aforementioned adsorbents are synthetized using not only a complex pathway including protection/deprotection steps, but also a larger excess of NMDG. As a result, their synthesis complexity and the overall costs result in a non-applicability at industrial level.

It can also be noted that CCBMG possess a monolayer capacity similar to the one owned by commercially available materials such as Amberlite IRA 743 and Dowex BSR-1. However, these resins are polystyrene based and therefore their surface is hydrophobic. As already demonstrated by *Sabarudin et al.*[17] chitosan based materials, being more hydrophilic, possess an enhanced kinetic rate of adsorption in comparison with styrene based materials such as Amberlite.

Another important property for the evaluation of the real potential of an adsorbent is the regenerability: in fact, the adsorbent must undergo regeneration without losing adsorption capacity throughout the different cycles. In order to evaluate the regeneration behaviour of the

Table 4: Characteristics of various adsorbents containing NMDG moieties reported in literature

Adsorbent	Base material	Q^0 (mg/g)	Reference
CCBMG	Chitosan	6.2	This work[62,63]
CCTS	Chitosan	35.1	16
CCTs-NMDG	Chitosan	22.7	17
Amberlite IRA 743	PS	3.1	15
Dowex BSR-1	PS-DVB	7.5	14
MCM-41	Ordered mesoporous silica	8.6	64

beads, a column was packed with the adsorbent and three cycles of adsorption and regeneration were carried out. Besides testing the reusability of CCBMG, which is a fundamental requirement for large scale industrial application of the adsorbent, this test is also useful to evaluate the behaviour of CCBMG in operation conditions that emulate the final application in a continuous apparatus. For this reason, it was chosen to use a solution with a concentration equal to 100 mg/L of boric acid, which is approximately the concentration that can be found in a seawater with high boron content.

It can be observed from the histogram in *Figure 25*, reporting boron removal in percentage with respect to virgin beads that CCBMG reduce their adsorption capability of 15% and 10% respect to the first cycle, probably because not all the adsorption sites have been regenerated by the passage of the acid solution. *Table 5* reports further experimental data: it can be observed that the removal percentage of boric acid remains restricted to a relatively narrow range (75-88%) in all the repetitions tested.

Table 5: Experimental data obtained by the regeneration test on a column packed with CCBMG. Cycle 1 was effectuated with virgin beads, while in cycles 2 and 3 were used regenerated beads one time and two times respectively.

Cycle	Contact time (sec)	[B(OH)3] after treatment (mg/L)	[B] after treatment (mg/L)	[B(OH)3] recovered (%)
1	158	12.0	2.1	88
2	145	24.9	4.3	75
3	169	20.9	3.6	79

Considering that WHO edge for boron in drinking water is 2.4 mg/L and that a solution treated with virgin CCBMG at the experimental conditions possess a boron concentration of 2.1 mg/L, it can be assessed that virgin CCBMG is able to cut down boron concentration under the required limit and may be applied to seawater purification. This is not true, under the experimental conditions chosen, for regenerated CCBMG, which only cut down the concentration up to 4.3 mg/L and 3.6 mg/L. It is therefore needed a higher packing height or lower flux rate in order to achieve the same percentage of removal if regenerated CCBMG rather than virgin CCBMG is used.
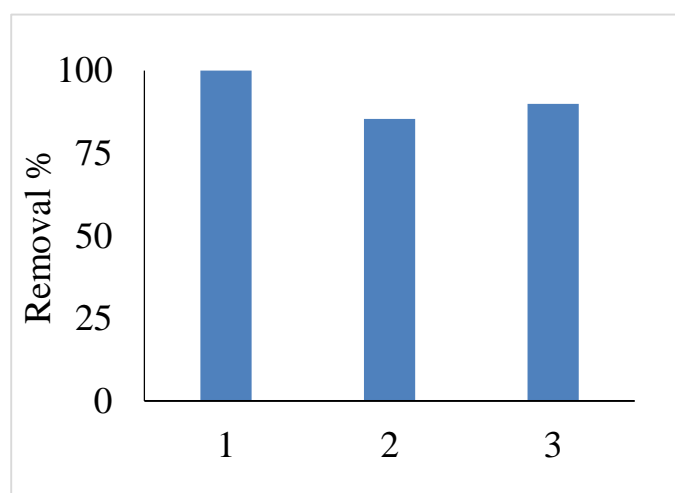

Figure 25: Removal percentage of CCBMG in a column dynamic test during three cycles of adsorption (1; 2; 3) and regeneration compared to the first cycle.

4.3. Membrane preparation

The porous membranes containing chitosan were prepared using $scCO_2$-assisted phase inversion. In order to apply this technique to produce a polymeric membrane, two basic requirements must be fulfilled: the first one is the possibility to solubilize the polymer in a solvent and the second is that the solvent must be miscible with $scCO_2$, so that it can be removed by fluxing continuously the SCF while precipitating the polymer.

In this work, the production of membranes containing chitosan, which can only be solubilized in acidified water, was studied. However, due to different polarity, water has a very limited solubility in $scCO_2$, and thus one of the aforementioned requirements is not satisfied. In order to make possible chitosan phase inversion, it is necessary to add an entrainer (in this case ethanol), which acts as a third component increasing the affinity between the solvent (water) and the non-solvent (carbon dioxide). Based on previous works[45] reported in literature it was chosen to add the entrainer to the non-solvent in isocratic mode and evaluate the influence of the composition of the casting solution and the depressurization time on the morphology of the membrane and, after the functionalization with NMDG, the efficiency in boric acid removal from aqueous solutions.

4.3.1. Membranes production: influence of the composition of the casting solution

The first experiments were conducted using a solution prepared dissolving chitosan 4% wt. in acetic acid 2% vol., producing the membrane (a) in *Figure 26*. As it is visible, the membrane is extremely thin due to the low amount of polymer present in the casting solution. This aspect, together with the brittleness of chitosan, which possess a glass transition temperature of 203

°C, confers poor mechanical resistance to the membrane. Consequently, membrane removal from the support was a problematic step, causing loss of integrity in the structure. The preparation of more concentrated chitosan solution was hindered by the formation of a viscous gel; to overcome the aforementioned limitation it was decided to blend chitosan with PVA in order to obtain a thicker and less brittle membrane.

Membrane (b) was produced from a 17% wt. solution. containing PVA/chitosan in an 87/13 ratio, while membrane (c) was produced from a casting solution containing 17% wt. of PVA. Comparing the two images, it is clearly visible that the composition of the casting solution has a major effect in determining the structure of the processed polymer: while membrane (b) is flat and homogeneous, membrane (c) has no regular shape resulting curly and corrugate.
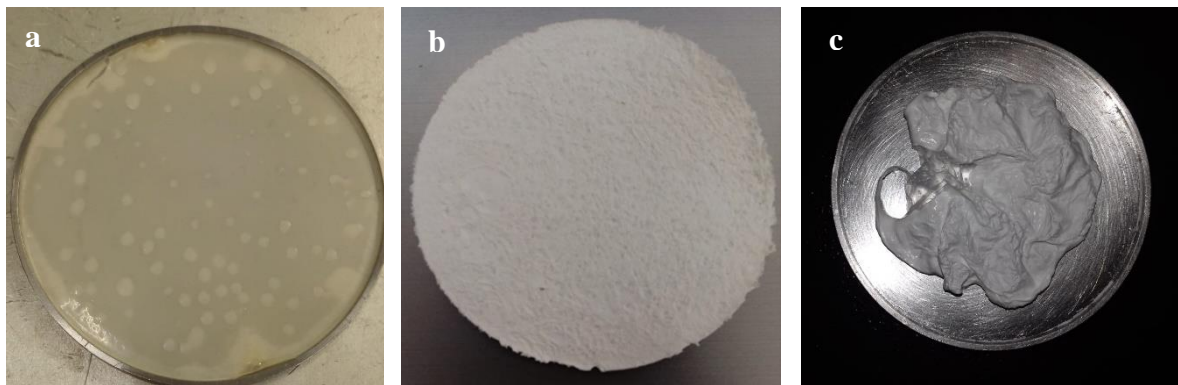

Figure 26:Membranes obtained from casting solutions possessing different composition: a) chitosan 4% wt.; b) PVA/chitosan 87:13 17% wt.; c) PVA 17% wt.

It was observed by visual inspection through the sapphire window of the high-pressure cell that loss of shape in membrane (c) takes place during the depressurization step. This evidence suggests that the plasticizing effect $scCO_2$ has on polymers lowers the glass transition temperature of PVA (80°C in normal conditions) under the experimental temperature determining the transition of the polymer to the rubbery state.

When depressurization starts, we expect to have CO_2 in the supercritical state not only inside the pores formed during phase inversion, but also adsorbed on the molecular chains of the polymer causing plasticization and swelling. As the pressure is reduced, the fluid starts diffusing outside the membrane. The diffusion through the pores is faster than diffusion through

the solid phase, meaning that the plasticization effect of the SCF on the polymer continues also if pressure is diminished. Nevertheless, the diffusion through the pores of the membrane causes pressure drops in the fluid, originating a gradient of pressure between the inner part of the membrane and the pressure on the cell. Such difference of pressure produces a stress in the membrane, and some pores inflate causing plastic deformation if the material is in the rubbery state. Hence, the membrane is subjected to a stress due to the diffusion of gaseous CO_2 outside of its structure.

PVA possess a relatively low T_g compared to that of chitosan (203 °C). As a result, the addition of chitosan results in the presence of material in the glassy state that makes the structure more rigid, and no plastic deformation is observed. On the contrary, pure PVA undergoes plastic deformation and the membrane shrinks creating a corrugated structure after CO_2 is removed.

A different explanation of the consistent difference between membranes (b) and (c) may be attributed to the different solubility of the two polymers composing the blend. In fact, chitosan is only soluble in acidic water, and the acetic acid used for the preparation of the solution possesses good affinity for the non-solvent, thus it is removed from the casting solution quickly. This causes the precipitation of chitosan, while PVA miscibility with the solvent varies with the amount of water removed from the non-solvent. Precipitated chitosan may act as nucleation site for PVA enhancing the phase inversion rate. As explained in a previous section, the precipitation rate strongly influences the structure of the final product. In particular, a higher rate gives origin to bigger pores; hence the PVA/chitosan membranes will have smaller pressure drops during the depressurization step and consequently a lower stress, determining no blowing effect.

It can be noted that in PVA/chitosan membrane the top skin layer is not dense and smooth but porous and rough. This phenomenon, explained by the fragile fracture of the surface pores that blow up in order to allow a faster diffusion of CO_2 outside of the system, will be discussed in detail in the next section.

Due to higher mechanical stability, facility of manipulation and uniformity, PVA/chitosan 87/13 membranes were chosen as starting material for subsequent studies.

4.3.2. Membranes functionalization

In order to confer to the membrane the properties required for the final application, the same functionalization reaction tested on the beads was used. The functionalization was performed in two steps. The aim of the first step is to crosslink the membrane in order to obtain an insoluble polymer and leave some epoxy functionalities on the surface of the pores. In the second step, taking advantage of the reaction of epoxides with amines, NMDG was grafted to the membrane.

Hence, for what it may concern the functionalization of the membrane, the discussion about the reaction mechanism is identical to the one previously reported for the beads, except that in this case also PVA possess –OH functional groups that may act as nucleophile for the first step of the reaction. Due to their large excess in comparison to the amino groups of chitosan, in this case hydroxyl groups are most likely the species that would react preferentially. Moreover, the temperature used in the reaction was reduced in comparison to the temperature of beads functionalization in order to limit PVA dissolution in water.

In order to confirm the success of the reaction this time it was not possible to use the ATR spectroscopy; in fact, being chitosan and NMDG present in much lower amount in comparison to PVA, no absorption peaks that may be attributed to their presence was found in the ATR spectra.

Hence, a CHNX elemental analysis was performed. CHN elemental analysis reports the weight percentage of some of the elements (nitrogen, carbon hydrogen) present in the sample. Comparing the percentage of nitrogen atoms in the functionalized membranes with the amount in the native membranes it is possible to confirm that the reaction has occurred. The results obtained are reported in *Table 6*.

Table 4: CNH elemental analysis data of non-functionalized (A; B) and functionalized (A NMDG; B NMDG) membranes.

Membrane	Depr. time	Nitrogen (%)	Carbon (%)	Hydrogen (%)	Moles of NMDG per gram
A	10 min	0.89	49.65	8.43	0
B	15 min	0.90	49.35	8.58	0
A NMDG	10 min	1.03	49.15	8.88	$7*10^{-6}$
B NMDG	15 min	1.06	49.42	8.85	$8*10^{-6}$

It can be observed that the functionalized membranes (the ones marked with the tag NMDG in the name) possess a higher percentage in nitrogen atoms than the native membranes, suggesting that NMDG has been grafted on the membranes.

The numbers of moles of NMDG added after functionalization was calculated using *Equation 5:*

$$N_{NMG} = \frac{X_f - X_u}{100 * M} \ (5)$$

Where:

N_{NMG} is the number of moles of NMDG added with the functionalization

X_f is the percentage of nitrogen atoms in the functionalized membrane

X_u is the percentage of nitrogen atoms in the non-functionalized membrane

M is the molar mass of NMDG

4.4. Membrane characterization: influence of depressurization time

4.4.1. SEM microscopy

It has been proven on previous research that the depressurization time has a major influence on the outcome of membrane morphology, and especially on the top layer[65]. Generally, whenever a membrane is produced using phase inversion technique, the top layer precipitates immediately after coming in contact with the non-solvent. As a result, a dense skin forms on the interface between the two phases. The aforementioned non-porous layer may limit diffusion and permeation in case of membranes used for filtration thus resulting in a disadvantage.

Using scCO$_2$-assisted phase inversion technique it is possible to overcome this limitation. In fact, this technique allows modulating surface porosity of the membranes throughout the application of small variations in depressurization time.

A visual evaluation of the membrane surface the was carried out by analysing SEM microscopy images. On figure 27 it can be noted an evident difference between the surface of the two native membranes: in fact while a depressurization time of 15 minutes results in the formation of porous cavities on the skin layer, a faster depressurization of 10 minutes causes the skin to disappear almost completely revealing the inner part of the membrane. In this case, it is therefore possible to have a homogeneous porosity throughout the section of the membrane, which is not possible to obtain using classic phase inversion techniques. In the SEM micrography of the native membrane surface produced with depressurization of 10 min, this aspect is clearly visible. In fact, it is possible to identify both the skin layer and the porous structure of the bulk.

Comparing the cross section images of the native membranes, differences in pore size and shape can be noted: in fact the membrane processed with a depressurization time of 15 minutes appear

more compact, with less pores of a smaller diameter. The explanation of this difference cannot be attributed to the precipitation mechanism, which is the same for both of the membranes. Consequently, being the only parameter varying between the two experiments, depressurization time influences again the pores morphology, this time on the bulk of the membrane. If a higher pressure gradient is applied taking advantage of a faster depressurization, the driving force of CO_2 diffusion outside of the membrane will be higher and a more consistent flux will originate. In order to equilibrate the stress caused, the membrane pores broaden in order to oppose less resistance to the flux. The mechanism is similar to the one allowing the foaming process: the decrease of T_g, consequence of the polymer swelling due to $scCO_2$, allows deformation of the structure. However, when CO_2 is removed the polymer shifts to the glassy state, freezing the deformation. As a result, in the membrane produced with 10 minutes of depressurization time it is possible to observe the presence of broad channels and a higher interconnectivity of the pores.

SEM analysis is also useful to observe the modification introduced on the morphology after functionalization, which was carried out in two steps, the crosslinking with epichlorhydrine and the grafting of N-methyl-D-glucamine. The main effect on the surface morphology appears to be a general diminution of the porosity. It can be noted, especially comparing the images of the membrane produced with 15 minutes depressurization time, that upon the surface of the membranes not only the number of pores is reduced, but also the mean diameter decreases.

A remarkable effect of an increase in the depressurization time can be also noticed in the micrographs of the cross section of the membranes, which appear denser and less porous. Moreover, while in the native membranes the pore walls possess an indented morphology, in the functionalized membrane their shape appears more rounded and smoother, probably due to the addition of material after crosslinking.

The average pore dimension is in the micrometric range; therefore, the membranes may be apt for implementation in microfiltration units for the pre-treatment of feed streams destined to RO plants, which is usually needed to remove suspended particles and in general macroscopic impurities.
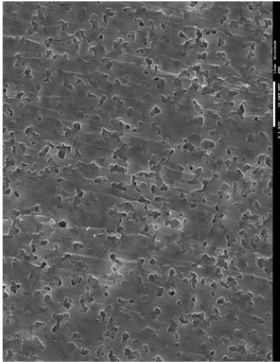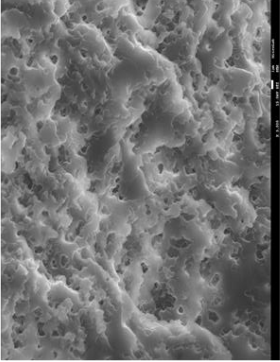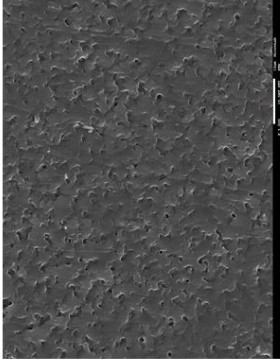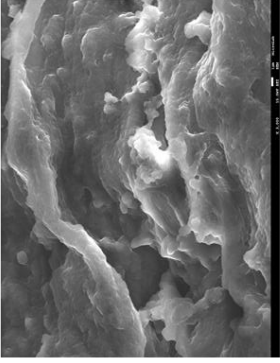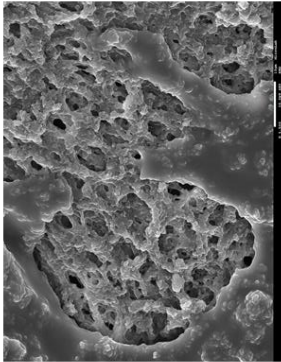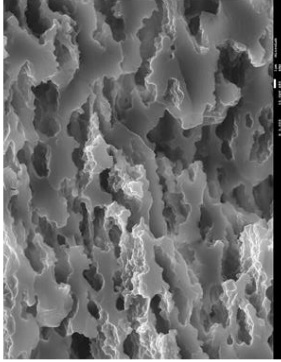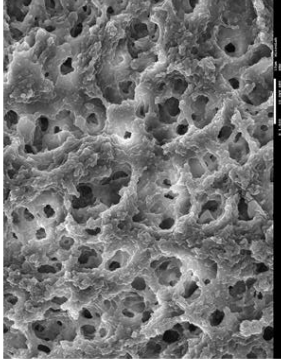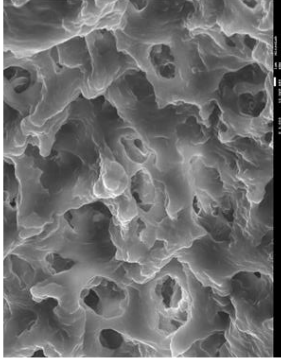
Figure 27: SEM microscopy images of the membranes. Surface images were recorded at 1500X magnifying factor, while cross section images were recorded at 3000X magnifying factor.

4.4.2. Flux measurement

One of the most relevant properties of a membrane defining the range of applicability is permeability. In fact, owing to the porous structure, a fluid is able to permeate through the membrane if a pressure is applied. The permeability is obtained plotting the flux of permeate measured by changes in the pressure applied. Normally, bigger and more interconnected pores would require a lower pressure in order to let the permeate flow.

Data obtained from permeability measurements on of PVA/chitosan membranes, reported in *Figure 28* and *Table 7*, evidence the major influence of depressurization time on the outcome of the membranes.

It can be noted that if no pressure is applied, then no flux is observed in both membranes. As pressure increases water contained in the cell starts to permeate. Nevertheless, permeation through membrane A (10 minutes) is much faster than through membrane B (15 minutes).

From SEM microscopy imagines it was possible to observe that the membrane produced with 10 minutes of depressurization time, besides possessing a more porous cross section are also missing the skin layer due to its blowing that creates pores to allow CO_2 to flow through. As a result, also the water flowing through the membrane is less hindered and the membrane possess a higher permeability value.

The enormous potential of morphology control that can be achieved taking advantage of scCO$_2$-assisted phase inversion can be noted by comparing the permeability values of membranes A and B: in fact, a variation of just five minutes in the depressurization time originates a difference in permeability of two orders of magnitude. By combining the regulation of other parameters such as pressure, temperature, composition of casting solution and non-solvent mixture, it is theoretically possible to strictly control the morphology of the polymer in order to obtain exactly the desired structure.

In order to confirm the suitability of the membranes for the implementation in a filtration unit, a fundamental requirement to be satisfied is the capability to bear the pressure applied. The operative pressure of a microfiltration unit ranges between 0.1 and 3 bar. *Table 7* reports the pressure at which the membranes have been tested. Membrane A has been tested applying maximum 1 bar, while membrane B has been tested applying a maximum of 4.6 bar. In the experimental conditions, no rupture of the membranes was observed and therefore it can be

assessed that both membranes may be used in a microfiltration unit for the pre-treatment of feed streams, which is usually included in RO plants in order to remove suspended particles and in general macroscopic impurities.
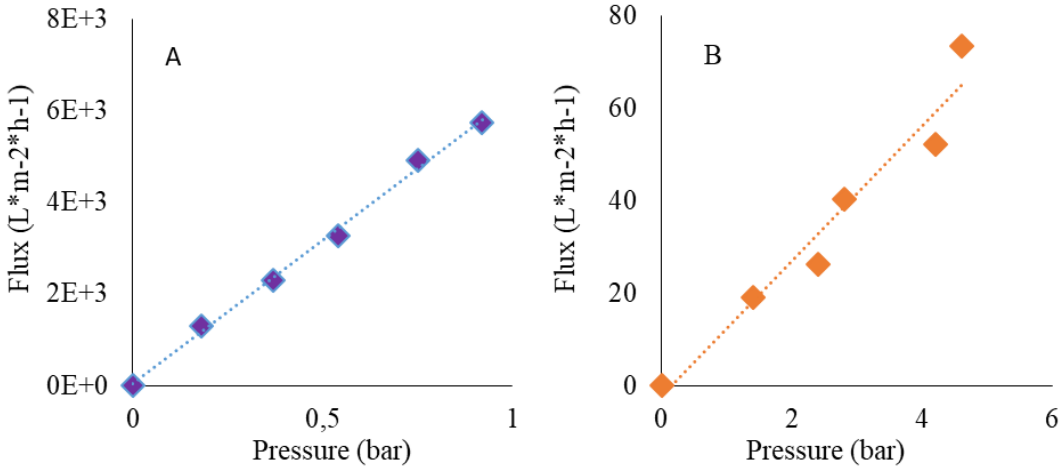

Figure 28: Permeability plot for membrane A NMDG (left) and B NMDG (right)

Table 7: Permeability values and operative pressure range for membrane A and B.

Membrane	Depressurization time (min)	Permeability (L*m^{-2}*h^{-1}*bar^{-1})	Pressure range (bar)
A	10	$6*10^3$	0-1
B	15	14	0-4.6

4.5. Adsorption and regeneration behaviour

By performing SEM analysis and permeability measurements, we showed that our membranes are suitable for the implementation in microfiltration systems for water purification.

Nevertheless, the main aim of this work is to produce a membrane to be used for the pre-treatment of aqueous feed of RO plants capable of removing boric acid from water. In order to confer this capability, the membranes were functionalized with NMDG, which forms a stable complex with boric acid at neutral pH.

The capability of boron removal was evaluated in the same stainless-steel filtration cell used for permeability measurements. The solution tested in the cell possessed a concentration of 50 mg/L of boric acid. Such concentration was chosen in order to test the membrane behaviour with a feed at the same boron concentration of a high boron content seawater.

The minimum pressure achievable with the laboratory equipment (0.1 bar approx.) was applied and the permeate was collected.

It is interesting to notice that, differently from the non-functionalized beads, which were not able to adsorb boric acid, the native membranes possess a good adsorption capability even without NMDG moieties. The reason may be due to the presence of hydroxyl groups in PVA chains forming borate esters.

Nevertheless, it can be noted that adding NMDG moieties to the membrane drastically increase boric acid complexation capability of the material. As explained in section 1.1.2, this effect is due to the presence of nitrogen atom in NMDG, which increases the kinetic and at the same time, by binding to the proton produced during the complex formation reaction, stabilizes the borate ester due his buffer behaviour and electrostatic interaction between protonated amine and negatively charged boron atom.

Given that both the functionalized membranes possess approximately the same quantity of NMDG moieties (see *Table 6*), the difference in adsorption capability reported in *Table 8* is due to the morphology of the membrane. In fact, in membrane A, which possess bigger pores and higher permeability, the filtration time is much shorter than the one in the experiment with membrane B.

Table 8: Experimental data of adsorption test membranes.

Membrane	Functionalization	$[B(OH)_3]$ permeate	$B(OH)_3$ removed (%)	Total time of filtration (sec)
A	None	29.23	41	360
B	None	11.65	76	405
A	NMDG	5.72	88	1020
B	NMDG	< LOD	100	3300

As a result, the contact time of the fluid with membrane A is shorter, meaning that there is less time for the complexation reaction to happen and less boric acid is removed from water.

Membrane B functionalized with NMDG possess the highest boron removal power: in fact, under the experimental conditions is able to adsorb 100% of the boric acid dissolved in solution, although the filtration is very slow due to the low permeability. In addition, even membrane A shows good retention properties: it is in fact able to remove 88% of boric acid. Nevertheless, the filtration with the aforementioned membrane yields a permeate with a concentration of boric acid of 5.72 mg/L, which is still higher than the limit of 2.4 mg/L suggested by WHO.

The histogram in *Figure 29* shows the removal percentage of boric acid in operative conditions.
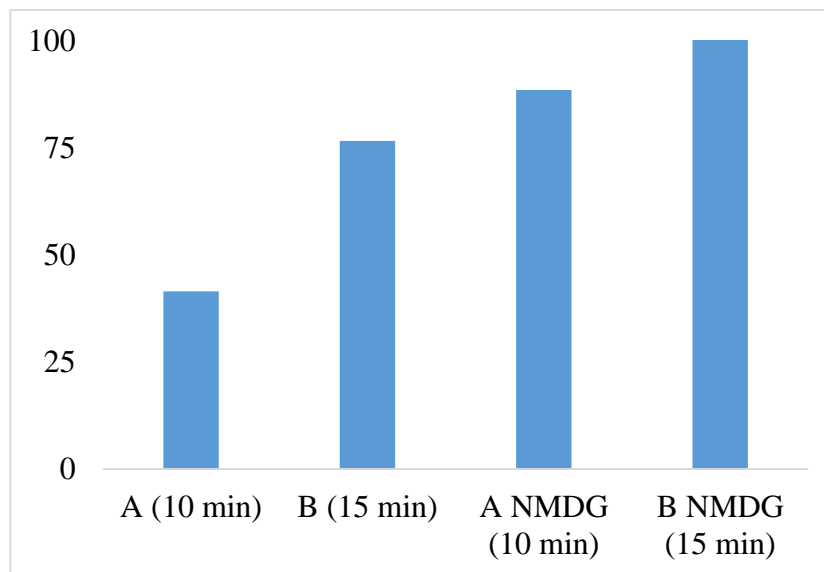
Figure 29: Boric acid removal percentage of the tested membranes from a solution 50 mg/L.

The possibility to regenerate a membrane is a fundamental requirement because it allows reusability and consequently increases the added value of the product. Moreover, recovered boric acid can be sold or implemented in different processes and the consequent reduction of wastes increases the overall sustainability of the process. It was chosen to carry out the regeneration test on membrane B NMDG due to its higher adsorption power.

If immersed in an acid solution, the borate ester formed by the hydroxyl groups on the surface of the membrane and boric acid can be broken and the membrane is regenerated. Nevertheless, it is important to verify that the regeneration process does not affect the membrane properties, causing loss of adsorption capacity. To do so, the adsorption test was repeated after the regeneration of the membrane. The histogram in *Figure 30* reports the boron removal percentage with respect of the first cycle, which was effectuated with the native membrane. It can be observed that the membrane reduces her adsorption capability of 17% in the second cycle and a higher loss of 56% is found after using the membrane a third time, probably due to membrane degradation after the immersion in the acid solution used for the regeneration.
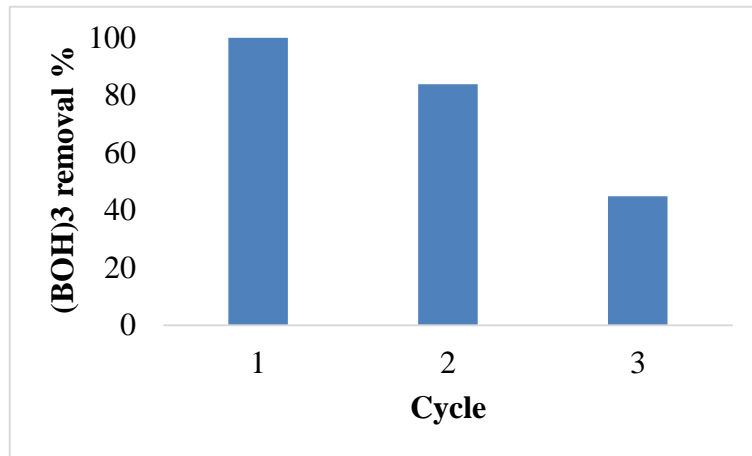
Figure 11: Regeneration behaviour of A NMDG. Adsorption capability of the membrane in percentage with regard to first cycle executed with the virgin membrane.

5. Conclusions

Boron is an essential element for the regulation of some biochemical reactions not only for humans and animals, but also for plants. However if assumed in high concentration it can cause several health problems including reduced fertility and damage to the nervous system in humans while it can decrease the growth rate and yield in plants. For this reason WHO suggested a limit of 2.4 mg/L for drinkable water.

In order to comply with WHO guidelines, water treatment systems able to remove boron must be implemented for example in waste treatment of effluents in metallurgic or glass industry and desalinization plants for the production of potable water from seawater.

Reverse osmosis (RO), which is the most commonly adopted method for effluent and seawater purification is only able to efficiently separate boric acid at basic pH but issues deriving from scaling on the membrane surface and costs of neutralization of the buffers used make the technique unapt. With the aim of removing boric acid it is generally used an additional pre-treatment system constituted by a boron selective resin in addition to the microfiltration unit which is always needed in order to remove macroscopic impurities before the use of a RO membrane. Nevertheless, boron selective resin possesses small capacity and slow kinetic of adsorption which should be improved to enhance the economic attractiveness of the process.

5.1. Beads

In the first part of this thesis, chitosan hydrogel beads were designed as an alternative for boron selective resins commercially available. Chitosan beads (CB) were produced by dropping a solution containing the polymer in a jellifying bath at basic pH. An optimization of the concentration of the polymer solution was required in order to obtain a spherical shape of the particles and it was found that the solution giving the best result was 2% chitosan. The beads formed with this technique possess a diameter between 400 and 800 μm and homogeneous shape.

In order to confer selectivity and higher adsorption capacity to the beads, N-methyl-D-glucamine (NMDG) was graft ed onto the surface of the beads. The grafting reaction used consisted in two steps: first the beads were treated with epichloridrine yielding cross-linked chitosane beads (CCB) and subsequently NMDG was grafted on the surface, producing cross-linked chitosane beand N-methyl-D-glucanine funzioncionalized (CCBMG). The cross-linking step accomplishes two roles: makes the beads insoluble even in acidic water and at the same time leaves on the surface of the beads some epoxy groups, which are the functional groups that react in the second step, binding NMDG. The synthesis pathway adopted in this work is shorter and easier than the ones used to produce analogous materials reported in literature[17,61]. ATR analysis was used in order to confirm that the functionalization reactions had happened successfully.

In order to evaluate if CCBMG possessed the required properties for the application in a water purification system, adsorption tests were performed in static mode in order to determine the influence of the adsorbate concentration. After suspending a weighted amount of CCBMG in solutions containing different concentrations of boric acid until the equilibrium is reached, the solutions were filtered and boric acid concentration was determined by the curcumin colorimetric method.

Data obtained was fitted in linearized Langmuir equation in order to obtain the monolayer adsorption capacity (Q^0), which was the parameter adopted in order to make comparisons between different adsorbents. It was found a value of Q^0 of 6.2 mg/g and 0.4 mg/g for CCBMG and CCB respectively. It was therefore demonstrated that the presence of NMDG moieties on the surface of the beads drastically increases the adsorption capability.

A comparison with adsorbents reported in literature was also effectuated, and it was found that CCBMG possess a lower adsorption capability than other analogous chitosan based adsorbents possessing NMDG moieties. However the synthetic pathway adopted in this work is more simple and sustainable, without any protection/deprotection steps and involves a lower consumption of chemicals. Q^0 value for CCBMG is found similar to the one possessed by Amberlite IRA 743, a commercially available boron selective resin. Nevertheless *Sabarudin et al.* [17] demonstrated that chitosan based adsorbent being more hydrophilic possess an higher adsorption rate than Amberlite, thus CCBMG can still be considered a valid material for boron removal from water.

The capability of the CCBMG beads of being regenerated was evaluated in dynamic mode by packing the adsorbent in a column. It was chosen to regenerate the column with a 0.5 M hydrochloric acid solution after fluxing in the column a solution containing boric acid. From the analysis of the boric acid solution, it was possible to evaluate the loss in the adsorption capability. It was found that after regeneration the beads loose between 10 and 15% of their initial adsorption capability for three successive cycles.

5.2. Membranes

The other boron selective adsorbent produced and presented in this work is in the form of a membrane. The membranes were produced by $scCO_2$-assisted phase inversion, which is a green and sustainable technique that presents some advantages in comparison with common organic solvent-based techniques. In fact, the use of $scCO_2$ as non solvent in phase inversion introduces additional parameters allowing to control the morphology of the porous structure.

In fact, if CO_2 is in the supercritical state close to the critical point, a small variation in temperature or pressure determines a consistent change in fluid density and diffusivity, thus resulting in a change in the solvent power.

Another tool to control the morphology is the depressurization step: in fact in order to have CO_2 in the supercritical state it is necessary to use high pressures. The rate at which pressure is released may have a major influence on the morphology of the membrane.

Firstly, the influence of the composition of the casting solution was evaluated. Three different solutions were prepared, one containing chitosan, one containing PVA and one containing a blend of chitosan and PVA. Although the membranes were produced with the same methodology, some important differences could be evidenced. In fact, chitosan membrane was thin and brittle, due to the low concentration of the casting solution that was possible to achieve (4% wt.) and the intrinsic rigidity of chitosan. PVA membrane was produced with a concentration of polymer in the casting solution of 17% wt., thus resulting in a thicker membrane. Nevertheless, pure PVA membranes shrink and undergo loss of shape during the depressurization step owing to the reduced rigidity of the polymeric chains, which are not able to bear the stress caused by the diffusion of CO_2. Finally, membranes possessing stable dimension and good mechanical resistance were produced starting from a blend solution of PVA/chitosan 83/17 wt. and this composition of the casting solution was adopted to produce the membranes used in the subsequent work.

Subsequently the work focused on the production of PVA/chitosan membranes with a controlled porosity. In order to obtain membranes possessing the requirements to be used in a microfiltration system, the control parameter chosen was the depressurization rate. Indeed two membranes were produced using depressurization time of 10 and 15 minutes.

In order to evidence the different morphology, SEM analysis was carried out. The images showed a great difference in the porosity and the compactness of the membrane, both in the surface and the cross section. While membranes produced with higher depressurization time possess a top skin layer and superficial porosity, in membranes produced with smaller depressurization time the skin layer is removed after the blowing of surface pores. Consequently, superficial morphology appear similar to the one in the cross section. A variation in membrane porosity due to depressurization time can also be noted in the cross section of the membrane: the smaller the depressurization time, the bigger and more interconnected are the pores formed.

In order to confer the membranes mechanical resistance, adsorption capacity and selectivity towards boric acid, a functionalization reaction with NMDG was effectuated. The reaction was carried out in two steps and involved crosslinking with ECH and grafting of NMDG. The addition of NMDG was confirmed by elemental analysis, which showed that the membranes possess between $7*10^{-6}$ and $8*10^{-6}$ moles of NMDG per gram. A comparison of SEM images of the native membranes with the functionalized ones showed that after the reaction the overall porosity is reduced thus resulting in a more compact membrane, not only in the cross section but also on the surface.

Further characterization was carried out by performing a flux measurement in order to determine permeability. Observations already reported after SEM analysis were confirmed: a longer depressurization time causes the formation of smaller and less interconnected pores, thus resulting in a lower permeability value. It was found that the membranes produced with 10 minutes and 15 minutes depressurization time possess a permeability to pure water value of $6*10^3$ and 14 ($L*m^{-2}*h^{-1}*bar^{-1}$) respectively. The difference of almost three orders of magnitude between the permeability values obtained by a variation of only 5 minutes of the depressurization time shows the high potential in controlling the morphology given by the technique adopted.

From the permeability measurement it was also confirmed that the membranes are able to bear the pressure required for the application in microfiltration systems.

The evaluation of the adsorption capability was effectuated in dynamic mode in order to emulate membrane behaviour in real operating conditions. A solution containing boric acid at a concentration similar to the one present in a seawater with high boron content was fluxed through the membrane and the concentration of boric acid in the permeate was analysed. It was

found that all the membranes possess a certain adsorption capacity even if not functionalized, nevertheless membranes containing NMDG moieties are better adsorbents and are able to cut down boron concentration under the edge suggested by WHO for drinking water.

Subsequently the investigation was carried out to verify the possibility to regenerate the membranes. It was found that under the experimental conditions the membrane lose 17% of the original adsorption capacity after one regeneration, while after the second regeneration the adsorption capacity drastically decrease at 56% of the original capacity.

However, given the high potential of the membranes produced and the peculiar characteristics of scCO$_2$-assisted phase inversion, which easily allows a strict control of the processed polymer morphology, it would be of relevant interest to address future research in the optimization of the process, aiming to obtain a system possessing an improved capability of regeneration.

6. References

[1] YASUDA, Seiji; YAMAUCHI, Hirotoshi. Recovery of boron from natural gas brines by chelating resins. *Nippon Kagaku Kaishi*, 1987, 1987.4: 752-756.

[2] NIELSEN, Forrest H. Is boron nutritionally relevant?. *Nutrition reviews*, 2008, 66.4: 183-191.

[3] DEVIRIAN, Tara A.; VOLPE, Stella L. The physiological effects of dietary boron. 2003.

[4] KOT, Fyodor S. Boron sources, speciation and its potential impact on health. *Reviews in Environmental Science and Bio/Technology*, 2009, 8.1: 3-28.

[5] KHALIQ, Haseeb; JUMING, Zhong; KE-MEI, Peng. The physiological role of boron on health. *Biological trace element research*, 2018, 186.1: 31-51.

[6] WORLD HEALTH ORGANIZATION, *Boron in drinking-water: Background document for development of WHO Guidelines for Drinking-water Quality*. Geneva: World Health Organization, 2009.

[7] EDITION, Fourth. Guidelines for drinking-water quality. *WHO chronicle*, 2011, 38.4: 104-8.

[8] POWER, Philip P.; WOODS, William G. The chemistry of boron and its speciation in plants. *Plant and Soil*, 1997, 193.1-2: 1-13.

[9] PIZER, Richard. Boron acid complexation reactions with polyols and α-hydroxy carboxylic acids: equilibria, reaction mechanisms, saccharide recognition. *Inorganica Chimica Acta*, 2017, 467: 194-197.

[10] YOSHIMURA, Kazuhisa, et al. Complexation of boric acid with the N-methyl-D-glucamine group in solution and in cross-linked polymer. *Journal of the Chemical Society, Faraday Transactions*, 1998, 94.5: 683-689.

[11] KITANO, Yasushi; OKUMURA, Minoru; IDOGAKI, Masatoshi. Coprecipitation of borate-boron with calcium carbonate. *Geochemical Journal*, 1978, 12.3: 183-189.

[12] FERREIRA, Odair Pastor, et al. Evaluation of boron removal from water by hydrotalcite-like compounds. *Chemosphere*, 2006, 62.1: 80-88.

[13] CHOI, Won-Wook; CHEN, Kenneth Y. Evaluation of boron removal by adsorption on solids. *Environmental Science & Technology*, 1979, 13.2: 189-196.

[14] HILAL, Nidal; KIM, G. J.; SOMERFIELD, C. Boron removal from saline water: a comprehensive review. *Desalination*, 2011, 273.1: 23-35.

[15] PARSAEI, Mahdi; GOODARZI, Mohsen Salarpour; NASEF, Mohamed Mahmoud. Adsorption study for removal of boron using ion exchange resin in batch system. In: *International Conference on Environmental Sciences and Technology IPCBEE*. 2011. p. 398-402.

[16] WEI, Yu-Ting; ZHENG, Yu-Ming; CHEN, J. Paul. Design and fabrication of an innovative and environmental friendly adsorbent for boron removal. *Water research*, 2011, 45.6: 2297-2305.

[17] SABARUDIN, Akhmad, et al. Synthesis of cross-linked chitosan possessing N-methyl-d-glucamine moiety (CCTS-NMDG) for adsorption/concentration of boron in water samples and its accurate measurement by ICP-MS and ICP-AES. *Talanta*, 2005, 66.1: 136-144.

[18] SHENVI, Seema S.; ISLOOR, Arun M.; ISMAIL, A. F. A review on RO membrane technology: developments and challenges. *Desalination*, 2015, 368: 10-26.

[19] HILAL, Nidal; KIM, G. J.; SOMERFIELD, C. Boron removal from saline water: a comprehensive review. *Desalination*, 2011, 273.1: 23-35.

[20] OO, Maung Htun; SONG, Lianfa. Effect of pH and ionic strength on boron removal by RO membranes. *Desalination*, 2009, 246.1-3: 605-612.

[21] TAGLIABUE, Marco; REVERBERI, Andrea P.; BAGATIN, Roberto. Boron removal from water: needs, challenges and perspectives. *Journal of Cleaner Production*, 2014, 77: 56-64.

[22] HASSON, David, et al. Scaling propensity of seawater in RO boron removal processes. *Journal of membrane science*, 2011, 384.1-2: 198-204.

[23] SMITH, Bryan M.; TODD, Paul; BOWMAN, Christopher N. Hyperbranched chelating polymers for the polymer-assisted ultrafiltration of boric acid. *Separation science and technology*, 1999, 34.10: 1925-1945.

[24] KABAY, N., et al. Adsorption-membrane filtration (AMF) hybrid process for boron removal from seawater: an overview. *Desalination*, 2008, 223.1-3: 38-48.

[25] KNEZ, Željko, et al. Industrial applications of supercritical fluids: A review. *Energy*, 2014, 77: 235-243.

[26] HOWARD, Henry; BILLINGHAM, John. Recycle for supercritical carbon dioxide. U.S. Patent Application No 10/274,302, 2003.

[27] CASIMIRO, Teresa, et al. Synthesis of highly cross-linked poly (diethylene glycol dimethacrylate) microparticles in supercritical carbon dioxide. *European polymer journal*, 2005, 41.9: 1947-1953.

[28] YUK, Hyun Gyun, et al. Nonthermal Processing of Orange Juice Using a Pilot-Plant Scale Supercritical Carbon Dioxide System with a Gas–Liquid Metal Contactor. *Journal of food processing and preservation*, 2014, 38.1: 630-638.

[29] DEL VALLE, José M. Extraction of natural compounds using supercritical CO2: Going from the laboratory to the industrial application. *The Journal of Supercritical Fluids*, 2015, 96: 180-199.

[30] KIRAN, Erdogan; DEBENEDETTI, Pablo G.; PETERS, Cor J. (ed.). *Supercritical fluids: fundamentals and applications*. Springer Science & Business Media, 2012.

[31] COOPER, Andrew I. Porous materials and supercritical fluids. *Advanced materials*, 2003, 15.13: 1049-1059.

[32] MARTINI, J. E.; ELLEN, J.; SUH, N. P. The Production and Analysis of Microcellular Foam, Master's Thesis. *Mechanical Engineering, MIT*, 1981.

[33] TEMTEM, Márcio Milton Nunes. Development of biocompatible and "smart" porous structures using CO2-assisted processes. 2009.

[34] GUILLEN, Gregory R., et al. Preparation and characterization of membranes formed by nonsolvent induced phase separation: a review. *Industrial & Engineering Chemistry Research*, 2011, 50.7: 3798-3817.

[35] SMOLDERS, C. A., et al. Microstructures in phase-inversion membranes. Part 1. Formation of macrovoids. *Journal of Membrane Science*, 1992, 73.2-3: 259-275.

[36] KHO, Yeh Wei; KALIKA, Douglass S.; KNUTSON, Barbara L. Precipitation of Nylon 6 membranes using compressed carbon dioxide. Polymer, 2001, 42.14: 6119-6127.

[37] TSIVINTZELIS, I.; PAVLIDOU, E.; PANAYIOTOU, C. Porous scaffolds prepared by phase inversion using supercritical CO2 as antisolvent: I. Poly (l-lactic acid). *The Journal of supercritical fluids*, 2007, 40.2: 317-322.

[38] REVERCHON, E.; CARDEA, S.; RAPUANO, C. Formation of poly-vinyl-alcohol structures by supercritical CO2. *Journal of applied polymer science*, 2007, 104.5: 3151-3160.

[39] REVERCHON, E.; CARDEA, S.; RAPPO, E. Schiavo. Membranes formation of a hydrosoluble biopolymer (PVA) using a supercritical CO2-expanded liquid. *The Journal of Supercritical Fluids*, 2008, 45.3: 356-364.

[40] TEMTEM, Márcio; CASIMIRO, Teresa; AGUIAR-RICARDO, Ana. Solvent power and depressurization rate effects in the formation of polysulfone membranes with CO2-assisted phase inversion method. *Journal of membrane science*, 2006, 283.1-2: 244-252.

[41] TEMTEM, Márcio, et al. Preparation of membranes with polysulfone/polycaprolactone blends using a high pressure cell specially designed for a CO2-assisted phase inversion. *The Journal of Supercritical Fluids*, 2008, 43.3: 542-548.

[42] TEMTEM, Márcio, et al. Supercritical CO2 generating chitosan devices with controlled morphology. Potential application for drug delivery and mesenchymal stem cell culture. *The Journal of Supercritical Fluids*, 2009, 48.3: 269-277.

[43] REVERCHON, E.; CARDEA, S.; RAPPO, E. Schiavo. Membranes formation of a hydrosoluble biopolymer (PVA) using a supercritical CO2-expanded liquid. *The Journal of Supercritical Fluids*, 2008, 45.3: 356-364.

[44] TSIVINTZELIS, I.; PAVLIDOU, E.; PANAYIOTOU, C. Porous scaffolds prepared by phase inversion using supercritical CO2 as antisolvent: I. Poly (l-lactic acid). *The Journal of supercritical fluids*, 2007, 40.2: 317-322.

[45] MUÑOZ, Ivan, et al. Life cycle assessment of chitosan production in India and Europe. *The International Journal of Life Cycle Assessment*, 2018, 23.5: 1151-1160.

[46] LIU, Hui, et al. Chitosan kills bacteria through cell membrane damage. *International journal of food microbiology*, 2004, 95.2: 147-155.

[47] HELANDER, I. M., et al. Chitosan disrupts the barrier properties of the outer membrane of Gram-negative bacteria. *International journal of food microbiology*, 2001, 71.2-3: 235-244.

[48] MENG, Xianghong, et al. Physiological responses and quality attributes of table grape fruit to chitosan preharvest spray and postharvest coating during storage. *Food Chemistry*, 2008, 106.2: 501-508.

[49] MENG, Xianghong, et al. Effects of chitosan and oligochitosan on growth of two fungal pathogens and physiological properties in pear fruit. *Carbohydrate Polymers*, 2010, 81.1: 70-75.

[50] MORGADO, Patrícia I., et al. Ibuprofen loaded PVA/chitosan membranes: A highly efficient strategy towards an improved skin wound healing. *Carbohydrate polymers*, 2017, 159: 136-145.

[51] TEMTEM, Márcio, et al. Dual stimuli responsive poly (N-isopropylacrylamide) coated chitosan scaffolds for controlled release prepared from a non residue technology. *The Journal of Supercritical Fluids*, 2012, 66: 398-404.

[52] KEAN, T.; THANOU, M. Biodegradation, biodistribution and toxicity of chitosan. *Advanced drug delivery reviews*, 2010, 62.1: 3-11.

[53] VAKILI, Mohammadtaghi, et al. Novel cross-linked chitosan for enhanced adsorption of hexavalent chromium in acidic solution. *Chemical Engineering Journal*, 2018, 347: 782-790.

[54] HUANG, Liqiang, et al. Poly (methacrylic acid)-grafted chitosan microspheres via surface-initiated ATRP for enhanced removal of Cd (II) ions from aqueous solution. *Journal of colloid and interface science*, 2013, 405: 171-182.

[55] WANG, Guanghui, et al. Adsorption of uranium (VI) from aqueous solution onto cross-linked chitosan. *Journal of hazardous materials*, 2009, 168.2-3: 1053-1058.

[56] BUNTON, N. G.; TAIT, B. H. Determination of boron in waters and effluents using curcumin. *Journal (American Water Works Association)*, 1969, 357-359.

[57] HATCHER, John T.; WILCOX, L. V. Colorimetric determination of boron using carmine. *Analytical chemistry*, 1950, 22.4: 567-569.

[58] SPENCER, Roberto R.; ERDMANN, David E. Azomethine H colorimetric method for determining dissolved boron in water. *Environmental Science & Technology*, 1979, 13.8: 954-956.

[59] HARDCASTLE, James Edward. A study of the curcumin method for boron determination. 1960.

[60] MOHAN, Thotegowdanapalya C.; JONES, Alexandra ME. Determination of boron content using a simple and rapid miniaturized curcumin assay. *Extraction*, 2017, 6247: 04.

[61] WU, Qiang; LIU, Mingyan; WANG, Xiong. A novel chitosan based adsorbent for boron separation. Separation and Purification Technology, 2019, 211: 162-169.

[62] FABBRI, Alessandro et al. N-methyl-D-glucamine Functionalized Chitosan Beads and Membranes for Boron Removal from Water

[63] FABBRI, Alessandro et al. Highly efficient chitosan beads and membranes for boron removal. PTIM2019, 2019, 193.

[64] KAFTAN, Öznur, et al. Synthesis, characterization and application of a novel sorbent, glucamine-modified MCM-41, for the removal/preconcentration of boron from waters. Analytica Chimica Acta, 2005, 547.1: 31-41.

[65] MORGADO, Patrícia I.; AGUIAR-RICARDO, Ana; CORREIA, Ilídio J. Asymmetric membranes as ideal wound dressings: An overview on production methods, structure, properties and performance relationship. Journal of Membrane Science, 2015, 490: 139-151.